Toward a theory of collective resource distribution: a study of a dynamic morphogenesis controller

Payam Zahadat[1,2] · Daniel Nicolas Hofstadler[2]

Abstract

Nature has various approaches to manage the collective distribution of resources. The division of a honeybee colony into subgroups, the formation of ant trails to food sources, and the spread of tree branches to optimize the access to light are some examples of collective decision making for resource distribution. This paper investigates collective distribution via an algorithm named vascular morphogenesis controller (VMC). This algorithm is inspired by plant morphogenesis that is a result of competitions between branches for shared resources, e.g., water and minerals. The algorithm acts on a directed graph and determines its dynamics over time. The nodes of the graph collectively decide on the distribution of a shared resource to propose the places to add or remove new nodes. The resulting dynamical system is adaptive to variations in the structural and environmental conditions. In this paper, the VMC is embodied in a modular physical structure. The structures' modules host the nodes of the VMC graph. They may suggest changes in the morphology over time, and a human can manually implement them into the physical structure. The paper investigates the effects of different parameters of the algorithm on the collective behavior of the system, both through embodied implementations and theory. The investigations have led to a better understanding of various aspects of the VMC and provided new knowledge to facilitate parameter selection for potential applications. Furthermore, the analyses have indicated similarities between the VMC and other types of collective systems, suggesting the potential benefits of viewing those systems from the perspective of resource distribution.

1 Introduction

Resource distribution is a collective process shared by many natural and artificial systems. Nutrients and other chemicals flowing in the vessels of plants, blood flowing in the vessels of

✉ Payam Zahadat
  payam.zahadat@uni-graz.at

1 REAL Lab, Computer Science Department, IT University of Copenhagen, Copenhagen, Denmark

2 Artificial Life Lab, University of Graz, Graz, Austria

animals, water flowing in river systems, information in the form of electrical signals flowing in neural networks or communication networks, and vehicles moving in road networks are examples of collective resource distribution systems. Often, the distribution of a resource across a complex system is an influential factor in its dynamics. Bejan and Zane (2012) suggest that the mechanisms of resource distribution are the principle elements of design in natural and engineered systems. He formulates the idea as follows: "for a finite-size system to persist in time (to live), it must evolve in such a way that it provides easier access to the imposed currents that flow through it." In this paper, we investigate a collective resource distribution algorithm, called vascular morphogenesis controller (VMC) (Zahadat et al. 2017b), to guide the dynamic morphology of a structure. The algorithm self-organizes the flows of a shared virtual resource and incorporates environmental conditions in the morphological dynamics of the structure.

In a distribution process, the term *resource* can be used as a general term to describe any given supply that is divided between several receivers. On the one hand, a swarm of active agents divided into subgroups, each focusing on a particular task, can be seen as a resource. An example is a swarm of honeybees divided into several task forces, i.e., foragers, nurses, etc. On the other hand, a set of tasks can be considered as a resource distributed among a number of agents, e.g., a set of orders from customers divided between the staff. The difference between the two examples resides in the way the problems are viewed, i.e., what is considered to be the fixed part and what is the more variable part of the system. In the first example, the honeybees replace each other over time, but the tasks often stay the same. In the second case, the orders vary, but the staff is often the same. In a path formation task (e.g., by ants) or in the development of branching structures (e.g., by slime mold), the active agents (e.g., ants or slime molds) are the resources distributed between different regions of the environment forming the paths of a network. The benefit of this general view of the term *resource* is to allow noticing similarities in the distribution mechanisms operating in various systems and to learn from those similarities.

The VMC algorithm studied in this paper abstracts plants' mechanisms of self-organized resource distribution. Individual branches of a plant compete for a shared resource distributed through a dynamic transportation network, i.e., the vascular system of the plant (Lucas et al. 2013). The shared resource (e.g., water, minerals, etc.) enters through the roots and flows toward the branches' tips, where it enables growth. The distribution of the resource at the branching points occurs relative to the vessel thicknesses of the branches. A hormone that is produced at the tips and flows rootward (opposite direction of the resource) is responsible for regulating the vessel thicknesses. The hormone is produced according to the local environmental conditions (e.g., light) and acts as a guiding signal, modifying the vascular system. Producing stronger flows of the hormone in a well-located branch results in thicker vessels between its tip and the root, and leads to more share of the resource and more growth for the branch. This positive feedback increases the plant's growth in the more favorable regions of the environment. However, the limitation of the shared resource imposes a negative feedback, restricting the size of the branching structure and the potential options for further growth. The resulting dynamic system can explore the environment, guide the morphology toward an optimized shape for the given environment, and adapt to future structural and environmental changes, e.g., a broken branch or a variation in the light conditions.

This paper extends the analysis and physical implementation of the VMC in Zahadat et al. (2018). A main contribution of this paper is the numerical analysis of the VMC dynamics that point to similarities between this system—that is explicitly designed for self-organization based on collective distribution of resource—and other types of multi-agent systems. Additionally, this paper presents physical experiments, as well as theoretical and simulation studies

on the behavioral effects of different parameterizations. VMC includes several parameters that determine different behavioral tendencies in terms of morphological dynamics and sensitivity to structural and environmental conditions. With the theoretical and numerical analysis of the parameters' effects, this paper provides a better understanding of how the system functions and gives a basis for parameter selection for future applications. The presented physical experiments provide a proof of concept, demonstrate the parameter effects in the real world, and support the predictions of the theoretical analysis. Similarities between the VMC and other types of multi-agent systems are the subject of the final part of the paper. These similarities suggest that the viewpoint of collective resource distribution is potentially beneficial in exploring and explaining some properties of different types of collective systems.

1.1 Related topics

1.1.1 Generation of forms

Regular repetitions of semi-identical forms in nature, for example on the outer skin of animals or nonlinear non-equilibrium chemical oscillators, e.g., the Belousov–Zhabotinsky reaction (Camazine et al. 2001; Goodwin 2001), can be described by reaction–diffusion mechanisms and Turing processes (Turing 1952). Many researchers (e.g., Devert et al. 2011; Murray 2003; dos Silva et al. 2015; Zahadat and Schmickl 2014) have widely investigated the formation of such patterns and their diversity and adaptability to environmental conditions. Morphogenetic models are often used to describe more complex patterns with multi-level hierarchies of forms. Morphogenesis is a generative process that uses the modular approach of repetition and variation. It usually starts with a few initial units and develops the system into a complex organism. The process is the result of interactions, both within the system and between the system and its environment. It is driven by the laws of physics, chemistry, and the information encoded in the genomes (Goodwin 2001). Several models have been proposed to develop artificial systems. Some models focus on cellular mechanisms such as variation of cell types, cell division, gene regulatory networks, and diffusion (Doursat et al. 2012). Some cellular automata models with various types of cells have also been implemented (Kowaliw and Banzhaf 2012). Other examples are L-systems (Lindenmayer 1975) that are abstract generative encodings introduced to describe the development of multi-cellular organisms, plants in particular. L-systems are formal grammars focusing mostly on the development of branching geometric structures by repetitive application of production rules on a set of symbols. Variations of L-systems have been used in developing artificial organisms (Hornby and Pollack 2001; Sims 1994). Researchers in mobile robotic swarms have employed various methods of self-organized morphogenesis. Most of those methods generate defined shapes and are mainly based on diffusion mechanisms, encodings of the desired shapes, and some form of rules determining the behavior of the robots (Meng et al. 2013; Rubenstein et al. 2014; Slavkov et al. 2018; Stoy and Nagpal 2007). The diffusion mechanism generates gradients providing information about the relative positioning of each robot. The robots react to this information by locating themselves according to their encoded rules concerning the desired shape. The gradient information can be used minimally and merely serve to differentiate between a seed robot and the rest (O'Grady et al. 2012). In most approaches to the morphogenesis of collective robots, the desired shape is well defined. Nevertheless, the shape can be loosely defined based on a set of requirements and preferences, e.g., the collective may prefer brighter regions of the environment over the darker ones (Divband et al. 2018a). The former approach is more similar to the embryogenetic mechanisms of animals. The

latter approach follows the mechanisms of plants (Sachs 1981), fungi (Bebber et al. 2007) and slime molds (e.g., *Physarum polycephalum*) (Nakagaki et al. 2000), strongly reflecting the environmental conditions in their self-organized shape. This more environment-oriented approach to morphogenesis has also been used in other areas of robotics, e.g., in soft robots (Laschi and Mazzolai 2016).

1.1.2 Resource transportation

Nature employs different mechanisms for resource transportation (Bejan and Zane 2012). When the environment shows a high resistance against transportation of a resource, *diffusion* is often the mechanism of transfer. Diffusion is a random walk of single particles resulting in a slow net flow down the concentration gradient. Another mechanism of transfer is the canalized motion of resources in a *transportation network*, where particles join their paths and form a mass flow down the pressure gradient of the medium. Transportation networks are mostly responsible for strong flows ensuring the fast distribution of resources. The morphology of transportation networks in some systems is a mere result of a flow gradient in the environment. For example, the formation of river systems is a result of the physics of fluids interacting with the environment. In biological systems, the branching patterns of transportation networks are often partially encoded in the genome (Goodwin 2001). The encoded information unfolds into a network structure via a modular process of repetition and variation of encoded forms. Some examples are the development of neural networks and vascular systems in animals and plants. The actual morphology of such networks is the dynamic result of the interactions of flows with their environment, plus the regional differences in the strengths of the flows. However, the formation of transportation networks in the world of living systems does not necessarily need a genetic encoding. Some of the examples are the formation of ant trails (Detrain and Deneubourg 2006), the growth of slime mold tubes (Nakagaki et al. 2000), and fungi (Bebber et al. 2007). In these examples, the flow networks are not genetically encoded. Instead, they are a direct result of interactions of agents among themselves, and with the environment. Several models describing the developmental mechanisms of such networks have been proposed and used as inspiration for solving problems in artificial systems. For example, pheromone trails connecting the nest of ants to patches of food (Detrain and Deneubourg 2006) have inspired optimization algorithms (Dorigo et al. 1996) and have been implemented in many robotic swarms (Campo et al. 2010; Payton et al. 2001; Sperati et al. 2011). The models mostly apply a reinforcement mechanism on the network connections based on the particle density (agent density) at the nodes. However, Ma et al. (2013) show that a flow-based reinforcement (according to the particle gradient of the connections) is preferable to the density-based reinforcement, leading to convergence to optimal shortest paths while automatically avoiding self-reinforcing loops.

1.1.3 Collective decision making

Collective decision making is the self-organized process of choosing some options over others. In many cases, the problem is to select among different areas in the environment to position the agents. There are several examples for such a process in nature, roughly dividable into two groups, i.e., spot selection and path selection. Examples of spot selection are nest site selection in honeybees (Seeley and Buhrman 2001), house hunting in ants (Franks et al. 2003), shelter selection in cockroaches (Halloy et al. 2007), and aggregation of young honeybees in regions of the hive with favorable temperature (Szopek et al. 2013). Examples of path

selection are path formation of ants between their nest and the best food patches (Detrain and Deneubourg 2006), growth of slime mold tubes toward regions with more food (Nakagaki et al. 2000), and growth of more branches in plants toward brighter regions (Sachs 1981). Still, further division of the mentioned groups is possible. For example, one can draw a rather loose line between the selection processes in a discrete set of spots (e.g., nest site, shelter, bridge, or branch) and in a continuous space of options (e.g., aggregating in preferable spots in a continuous temperature field, forming a path or a tube in a continuous environment). Despite their differences, all the various groups share the behavior of collectively selecting between different options. In this paper, we investigate an algorithm inspired from plants implementing a variation of the path selection behavior, i.e., to favor the growth (and further branching) of branches that are better positioned (wrt. light, gravity, etc.) compared to their mates.

1.1.4 Multi-agent systems

In multi-agent systems, complexity arises from local interactions. They span from swarm intelligence (Bonabeau et al. 1999) initially inspired by behaviors of social insects, via swarm robotics (Dorigo et al. 2014; Hamann 2018b), distributed approaches in microeconomics and market-based methods (Clearwater 1996; Deconinck et al. 2015; Kurose and Simha 1989). A common subject of interest shared in all these fields of research is resource distribution that includes task distribution and division of labor (Bonabeau et al. 1999; Huberman and Hogg 1995; Waldspurger et al. 1992; Zahadat et al. 2015; Zahadat and Schmickl 2016). Individual agents in a swarm consume or contribute to the shared resource while trying to meet their own private needs. Sharing common resources puts constraints on the swarm and imposes interdependencies between its agents. The interdependencies become more prominent where agents' reactions to their available resources are nonlinear. For instance, in an example scenario, the agents who receive a tiny share of the resource (below a threshold) may leave the swarm. In this case, a mechanism that maintains a uniform resource distribution can protect the swarm from shrinking, as long as the overall resource is enough. The interdependencies induced by resource sharing point to the importance of distribution mechanisms in steering the behavior of swarms, e.g., as in microeconomics and market-based control (Clearwater 1996; Kurose and Simha 1989). Similar topics and challenges also appear in the study of task allocation mechanisms and division of labor, e.g., how to distribute agents—the shared limited resource of the system—to handle sets of given tasks (Bonabeau et al. 1997; Karsai and Schmickl 2011; Pini et al. 2013; Zahadat et al. 2015).

1.2 Previous works on VMC

The VMC has been implemented previously in a number of different systems in simulation and in physical mobile robotic scenarios. In Zahadat et al. (2017b), an earlier version of VMC was evolved to grow structures in a physics-based simulation in different conditions (e.g., harsh and mild environmental conditions, different lighting). In Zahadat et al. (2017a) the behavior of VMC was demonstrated in a maze scenario, showing the preference for the shortest path. The controller has also been used for the growth of a non-deterministic structure in an architectural framework with interactive evolution (Heinrich et al. 2018). A variation of VMC with a root that is allowed to move within the network was implemented in Zahadat and Schmickl (2017, 2018), showing an amoeboid locomotion toward the source of interest. The algorithm has also been studied to show self-adaptation and self-repair in simulation

(Zahadat 2019) as well as physical mobile robotic systems. In the physical implementations, a swarm of mobile robots running VMC show adaptive path formation from a fixed root toward brighter regions of the environment and self-repair of the structure after damages (Divband et al. 2018a, b).

1.3 Physical implementation

In this paper, several experiments are conducted with the VMC embodied in physical structures. The traditional technique of braiding is employed in order to build autonomous structural modules that can be manually attached to (or detached from) each other.[1] The modules provide support and hold local electronics, i.e., sensors and processors. Every module acts as an autonomous agent. Once the modules are connected, the neighboring processors communicate to form a network of nodes that collectively decide how the shape of the structure should change. The VMC running in the network combines sensory information, intrinsic tendencies (e.g., exploration vs. exploitation) encoded as the parameters of the algorithm, and structural constraints (i.e., size). In the experiments, local light intensities and tilting of individual branches of the structure act as the local sensory information for each VMC node. The VMC network suggests where the structure must grow or shrink, with a tendency to grow upward and toward more light. If the nodes collectively decide on the addition or removal of a module, a signaling light at the position of the required change communicates it to the human. In practice, the human can deviate from the suggestions of the system and make their own changes to the structure. Likewise, the structure might change due to external reasons (e.g., a branch might be accidentally bent by a human passing by). In such cases, the collective distribution system adapts to the new conditions and presents new suggestions.

2 Vascular morphogenesis controller: a model of collective decision for resource distribution

Vascular morphogenesis controller (VMC) is a distributed algorithm inspired by the mechanisms of branching and growth in plants. All the branches of a plant share the necessary resources for growth. In this respect, they act as autonomous agents competing for the limited shared resource. To participate in the competition, each branch produces some amount of a hormone, called auxin (Leyser 2011), according to the local environment (e.g., the intensity of light received at the tip of the branch). The auxin hormone flows from the tips of the branches along the vessels toward the roots of the plant. On their way to the root, the hormones change the quality of the vessels, i.e., their capacity to transfer resources. According to the *canalization* hypothesis (Bennett et al. 2014; Sachs 1981), a well-positioned branch (wrt. environmental resources, e.g., light) produces high amounts of auxin which leads to better quality of vessels and therefore a higher share of the common resources and eventually more growth for the branch. Growth may facilitate the access of the branch to even better regions of the environment (e.g., more light) and lead to a positive feedback loop of better local conditions, a higher share of the resource, and more growth. Nevertheless, a higher share of the limited resource for well-positioned branches means a lower share is available for distribution among the others. Biological tissues generally deteriorate if no constant investment is made to keep them functional. Therefore, a non-successful (outcompeted) branch will be slowly

---

[1] In the context of the EU-funded project *flora robotica* (Hamann et al. 2017).
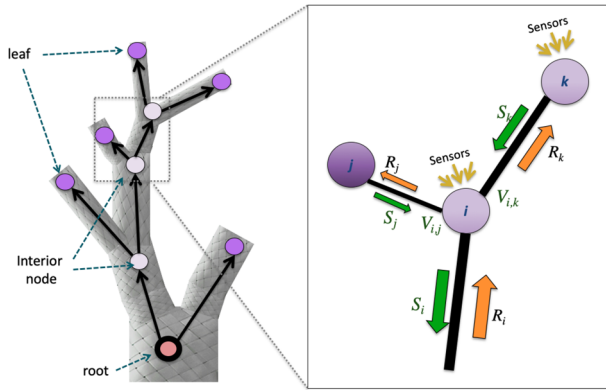
Fig. 1 An example structure guided by VMC. The VMC uses two flows: one flow, namely successin, starts at the leaves flowing toward the root and is responsible for the adjustment of the vessel thicknesses (connections of the graph). The production of successin at the leaves and its modification at the interior nodes are according to local environmental conditions perceived by the sensors and a set of constant parameters. The other flow, namely resource, starts at the root and flows toward the leaves being divided proportionally to the thickness of vessels. The resource motivates growth at the leaves

depleted of resources and eventually die.[2] The level of competition between branches can be fine-tuned globally depending on the availability of resources, which is reflected in hormonal status (Crawford et al. 2010; Domagalska and Leyser 2011). The self-organized distribution of the limited resource between the competing branches of a plant drives a collective process of decision making for finding favorable regions of the environment and to enable the plant to benefit growing in those regions.

The VMC abstracts the above-mentioned dynamics of the collective system in the growth process of an acyclic directed graph. Figure 1 summarizes this process in a schematic representation of an example VMC graph. The figure shows the flow of a value we call successin (in analogy to auxin in plants). Successin (S) is produced at the leaves of the graph and propagating toward the root. The flow of successin regulates the thickness of vessels (i.e., the weights of the connections of the graph). A limited shared resource (R) starts at the root of the graph and is distributed between the children of each node proportional to their vessel thickness (V). Real plants usually have only a single-root system (Morris et al. 2017). In a VMC graph, the *root node* represents the totality of a plant's root system. However, in nature there are cases where the shoots of multiple plants may fuse together, resulting in multiple root systems. Likewise, the acyclic directed graph of VMC is allowed to have multiple root nodes. Nevertheless, in all implementations of VMC presented here, the graphs only contain a single root. VMC graphs may expand through growth at their leaf nodes, i.e., by addition of new nodes to the leaves (in analogy to the outgrowth of new branches in plants). Similarly, the graph may lose some of the leaves (roughly analogous to the death, i.e., shedding, of branches in real plants).

In plants, auxin production occurs at the growing tips of branches according to the local conditions and parameters encoded in the genome. In analogy to that, successin production occurs at the leaves of the VMC graph according to the local sensory inputs and a set of

---

[2] The reduction in transport capacity caused by this neglect (i.e., the canalization of nutrients to better competitors) is reversible only up to a certain point. Beyond that point, some materials from the affected branch can be recycled back to the main stem in a process known as "senescence" and eventually, the branch will be shed ("abscission") (Sachs 2004).

constant parameters[3]:

$$S_{\text{leaf}} := \text{PRODUCTION}(\text{params, sensors}) \tag{1}$$

Successin flows toward the root, passing through interior nodes. At an interior node, a transfer function (in the range of $[0, 1]$) may alter the flow based on the local sensory inputs and constant parameters.

$$S_{\text{non-leaf}} := \text{TRANSFER}(\text{params, sensors}) \sum_{b \in \text{children}} S_b. \tag{2}$$

The local sensors used in the interior nodes might be different than those on the leaf nodes.

The successin passing a connection (i, j) of the graph (a vessel) adjusts its weight (thickness) according to a set of parameters, influencing the intensity of competition between the siblings:

$$V_{i,j} := V_{i,j} + \alpha \left(S_j^{\beta_i} - V_{i,j} \right), \quad \text{with} \quad \beta_i = \text{COMPETITION}(\text{params, sensors}), \tag{3}$$

where $V_{i,j}$ is the weight of the connection between node i and its child node j, S_j is the successin of node j flowing toward i, and α is the adaptation rate determining the speed of convergence of $V_{i,j}$ to $S_j^{\beta_i}$.

In the current work, the above-mentioned functions are implemented as follows. The production of successin at a leaf is defined as:

$$\text{PRODUCTION}(\text{params, sensors}) = f \left(\omega_c + \sum_{s \in \text{sensors}} \omega_s I_s \right), \tag{4}$$

where $f(x) = \max(0, x)$, ω_c is the constant term for production of successin at a leaf and ω_s is the sensor-dependent production term (a coefficient) determining the dependency of successin production on the sensor input I_s.

The transfer rate of successin passing an interior node is defined as:

$$\text{TRANSFER}(\text{params, sensor}) = g \left(\rho_c + \sum_{s \in \text{sensors}} \rho_s I_s \right), \tag{5}$$

where ρ_c is a constant transfer rate, ρ_s is the sensor-dependent transfer rate for sensor s, and $g(x) = \max(0, \min(1, x))$.

The intensity of competition is defined as:

$$\text{COMPETITION}(\text{params, sensor}) = \beta_c + \sum_{s \in \text{sensors}} \beta_s I_s, \tag{6}$$

where β_c and β_s, respectively, represent the constant competition term and the sensor-dependent competition term for sensor s.

Each of the above parameters can be set to zero according to the requirements of a particular application.

---

[3] In all the following equations, the operator := stands for the assignment of the right-hand side statement to the left-hand side variable occurring in every timestep.

2.1 Distribution of resource over the whole structure

A limited shared resource starts at the root, being distributed within the structure according to the thickness of the vessels (weight of the connections of the graph). A part of the resource reaching node i (R_i) can be consumed there. The remaining amount is divided between its children proportional to the thickness of their vessels. A given child j with vessel thickness $V_{i,j}$ receives

$$R_j := (R_i - c) \frac{V_{i,j}}{\sum_{b \in \text{children}} V_{i,b}}, \tag{7}$$

where c is the constant consumption term, representing the resource consumed at every non-leaf node, and *children* is the set of children of node i (including j). The parameter c can be set to zero.[4] In that case, all resource is divided only among the leaves of the graph (where new growth can happen). The amount of resource at the root node can be constant. Alternatively, it can be a function of the environment and the amount of successin that reaches the root. In the current implementation, R_{root} is fixed to a constant value.

2.2 Addition of nodes

A graph can grow at its leaves. Growth here means the addition of new leaves as the children of an old one. The decision about the occurrence of growth on a particular leaf follows a strategy that considers the amount of resource reaching it. An example strategy is to use a threshold th_{add} on the resource value at the leaf, determining whether or not growth should occur there. Another example strategy is to regard the resource at the leaves as the probability of growth. In such implementations of the growth strategy, the ratio between the resource consumption of nodes (c) and the total resource value (R_{root}) constrains the overall size of the graph.

2.3 Deletion of nodes

A deletion strategy can be defined for removing leaves from a VMC graph. The strategy may consider the amount of resource reaching the nodes and a threshold value th_{del}. For example, if all children of node i are leaves and $R_i < \text{th}_{\text{del}}$, the children can be removed and the node becomes a leaf. Alternative strategies may additionally include probabilistic and environmental factors. However, one can implement a growth process without any deletion.

3 Analysis of parameter effects

In this section, we apply a formal approach to analyze the effects of various parameters of VMC on the behavior of the structures. Table 1 presents the set of parameters in a VMC system and their descriptions. The focus here is solely on the effects of internal parameters. Therefore, in all setups, the sensor values are identical everywhere, unless stated otherwise.

---

[4] Considering the consumption of resource in plants, nutrients primarily aggregate at the growth zones (e.g., tips of branches and expanding leaves). The living cells of the vessels have only very small amounts of energetic "upkeep costs." In general, the consumption term will vary with the material to be consumed (e.g., water or nutrients), the tissues considered and the developmental or ecological situation.

Table 1 List of parameters

| Parameter	Description
α	Adaptation rate of vessels
β_c	Competition intensity between sibling vessels, constant
β_s	Competition intensity between sibling vessels, sensor-dependent
ρ_c	Transfer rate of successin at the interior nodes, constant
ρ_s	Transfer rate of successin at the interior nodes, sensor-dependent
ω_c	Production of successin at the leaves, constant
ω_s	Production of successin at the leaves, sensor-dependent
c	Consumption of resource in every node
R_{root}	Constant resource value at the root
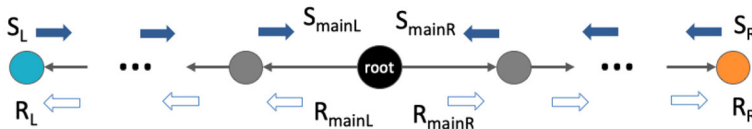
Fig. 2 An example one-dimensional VMC graph

The analysis demonstrates: (1) the intrinsic tendency of VMC toward favoring shorter paths, (2) the necessary conditions for overcoming this tendency and promoting asymmetry in equal conditions, and (3) the use of sensor-dependent transfer rate in reaching different growth behaviors in different branches.

In the following and where applicable, the TRANSFER and COMPETITION functions are represented by ρ and β, respectively.

3.1 Intrinsic tendency toward shorter paths

A simplified one-dimensional VMC structure is used to show the intrinsic tendency of VMC for choosing the shortest paths (see Fig. 2). In this setup, only the root node has two children. All other nodes have a single child at most. The lengths of the paths between the leaves and the root are n and m for the left and the right leaf, respectively. The sensor-dependent parameters for transfer and competition are set to zero ($\rho_s = \beta_s = 0$). To compute the successin for any non-leaf node of the structure, Eq. 2 can be rewritten as:

$$S_{\text{non-leaf}} := \rho \sum_{b \in \text{children}} S_b \tag{8}$$

Considering that there is only a single leaf on each side of the structure (Fig. 2), the successin reaching the root from one side, say the right side with the length m, converges to:

$$S_{\text{mainR}} = \rho S_2 = \rho^2 S_3 = \cdots = \rho^{m-1} S_m = \rho^m S_R \tag{9}$$

The same holds for the left side (with length n), and thus:

$$S_{\text{mainL}} = \rho^n S_L, \qquad S_{\text{mainR}} = \rho^m S_R \tag{10}$$

According to Eq. 3, and with a competition intensity β, the vessel thicknesses for the two branches of the root converge at the steady state to[5]:

$$V_{\mathrm{mainL}} = S_{\mathrm{mainL}}^{\beta} = (\rho^n S_{\mathrm{L}})^{\beta}, \qquad V_{\mathrm{mainR}} = S_{\mathrm{mainR}}^{\beta} = (\rho^m S_{\mathrm{R}})^{\beta} \qquad (11)$$

With a resource value of R_{root} at the root, due to Eq. 7 for resource distribution, the children of the root get the following amounts of resource:

$$R_{\mathrm{mainL}} = (R_{\mathrm{root}} - c)\frac{(\rho^n S_{\mathrm{L}})^{\beta}}{(\rho^n S_{\mathrm{L}})^{\beta} + (\rho^m S_{\mathrm{R}})^{\beta}}, \, R_{\mathrm{mainR}} = (R_{\mathrm{root}} - c)\frac{(\rho^m S_{\mathrm{R}})^{\beta}}{(\rho^n S_{\mathrm{L}})^{\beta} + (\rho^m S_{\mathrm{R}})^{\beta}},$$
$$(12)$$

Since there is no branching for any node except the root, the resource from every parent to its child equals the amount it receives minus the consumption c. Thus, the resource value at every leaf converges to:

$$R_{\mathrm{L}} = R_{\mathrm{mainL}} - n \cdot c, \quad R_{\mathrm{R}} = R_{\mathrm{mainR}} - m \cdot c, \qquad (13)$$

Combining Eqs. 12 and 13, the resources at the leaves are as follows if $S_{\mathrm{L}} = S_{\mathrm{R}}$:

$$R_{\mathrm{L}} = RC \cdot \rho^{n\beta} - n \cdot c, \qquad R_{\mathrm{R}} = RC \cdot \rho^{m\beta} - m \cdot c \qquad (14)$$

with $RC = (R_{\mathrm{root}} - c)/(\rho^{n\beta} + \rho^{m\beta})$.

Considering that $\rho \leq 1$, Eq. 14 means that the leaf with the shorter path to the root receives a higher share of the resource and therefore is more motivated to grow, except in the special case of $\rho = 1, c = 0$, where there is no preference. Where all conditions are equal, the preference for growing at the shorter paths leads to symmetric structures, because their growth continues until they reach the same length as others. This preference for shorter paths has been demonstrated previously in a case study of a maze scenario in simulation of a VMC-controlled organism (Zahadat et al. 2017a).

3.2 Effect of the sensor-dependent transfer rate in regulating the growth of particular branches

In the previous example, the transfer rate ρ was identical in all nodes. That was achieved by the use of a constant transfer rate and setting the sensor-dependent transfer rate to zero in Eq. 5. However, this is not necessarily the case in all scenarios. For instance, one can use light sensors at the leaves to influence the production rate of successin, and accelerometers (providing the tilting angle of branches) or stress sensors (associated with physical joints) at the interior nodes for influencing the transfer rate ρ. In the structure of Fig. 2, if $S_{\mathrm{L}} = S_{\mathrm{R}}$ and $m = n$ (see Eq. 14), high stress or bending that influences an interior node at the left branch can decrease the ρ of that node and lead to $S_{\mathrm{mainL}} < S_{\mathrm{mainR}}$ and consequently $R_{\mathrm{L}} < R_{\mathrm{R}}$, which results in a preference for growth at the right branch.

3.3 Combined effect of the number of nodes, competition intensity and transfer rate

Figure 3 shows an example VMC graph with n children for each non-leaf node. Let's assume that all the leaves of the left branch (represented in blue) have the same sensor values and
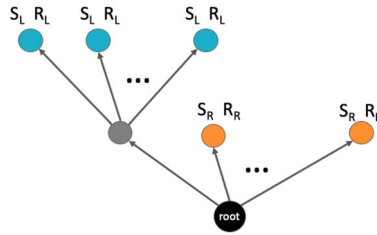
Fig. 3 An example VMC graph, where the root and its leftmost child each have n children. The thickness of the connections between the root and directly connected leaves is V_{R1}. The vessel thickness for the connection between the root and the only interior node of the graph is V_{L1}, and for all connections between the interior node and its n children is V_{L2}

consequently the same successin production S_L, all the others (represented in orange) have the same successin production S_R and, to simplify the equations, $c = 0$.

At the steady state, i.e., when the values converge, the successin passing the interior node is $S_{L1} = \rho n S_L$ according to Eq. 2 and the thicknesses of the vessels computed by Eq. 3 are:

$$V_{L2} = S_L^{\beta}, \quad V_{R1} = S_R^{\beta}, \quad V_{L1} = (n S_L \rho)^{\beta} \tag{15}$$

According to Eq. 7, the resources reaching a leaf on the left and right branch, respectively, are:

$$R_L = \frac{R_{root}}{V_{sum}} n^{\beta-1} (S_L \rho)^{\beta}, \quad R_R = \frac{R_{root}}{V_{sum}} S_R^{\beta}, \tag{16}$$

where $V_{sum} = V_{L1} + (n-1) V_{R1}$ is the sum of all the vessel thicknesses at the root node, R_L is the resource reaching a leaf of the left branch, and R_R is the resource reaching one of the other leaves.

Thus, the ratio between the resources depends on the ratio between their successin, the competition and transfer rates, and the value of n, as follows:

$$\frac{R_L}{R_R} = n^{\beta-1} \rho^{\beta} \left(\frac{S_L}{S_R}\right)^{\beta} \tag{17}$$

In an environment with $S_L = S_R$, the resource ratio is $\frac{R_L}{R_R} = n^{\beta-1} \rho^{\beta}$. It indicates that, if β is large, the structure tends to grow at branches with more nodes, and conversely, if ρ is small, tends to grow at shorter branches.

To prefer growth at the large branches, $n^{\frac{1-\beta}{\beta}} < \rho$ is a necessary condition. Considering that $\rho \leq 1$, the above condition never holds for $\beta \leq 1$. Hence, if the nodes are in equal states, with a $\beta \leq 1$ (as a sufficient condition), the structure always tends to grow symmetrically. On the other hand, since $n > 1$, $\frac{1}{\beta} > 0 \Rightarrow n^{\frac{1}{\beta}} > 1$, the following holds:

$$\frac{1}{n} < \frac{n^{\frac{1}{\beta}}}{n} = n^{\frac{1-\beta}{\beta}} < \rho \tag{18}$$

Thus, the preconditions for the tendency to grow at larger branches (i.e., toward asymmetry) are $\rho > \frac{1}{n}$ and $\beta > 1$.
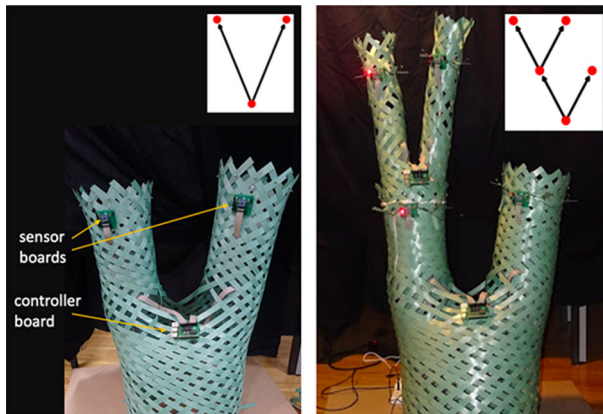
Fig. 4 An example braided module (left), and two connected modules (right), with their overlaid VMC graphs (inset images)

4 Experiments with physical structures

This section presents a set of experiments on physical structures, running VMC on distributed electronics. The experiments are designed to demonstrate parameterization effects similar to those discussed in the previous section but in physical setups.

4.1 Physical setup

The building blocks of the structure are Y-shaped braided modules, each augmented with a main board mounted on the base of the braid, two sensor boards mounted on the two branches, and a set of sensors. The sensor boards are connected to the main board, and each manages four light sensors and an accelerometer. The main board of a module often runs a single VMC node. One can connect the modules by attaching the base of one to a branch of another, making the former module a child of the latter (see Fig. 4). If a branch is not connected to a child module, the main board additionally runs a leaf VMC node as a child of its main node. Since each module has two branches, a node may have two leaf children at most. The sensor boards of the parent module are responsible for maintaining communication between the main boards of the parent and its children. Once a branch is ready for growth or removal, it signals the humans via LEDs located on the sensor boards. The human, in turn, manually realizes the change to the structure (addition/removal). The implementation details of the braided modules are described in Hofstadler et al. (2018). In short, the VMC graph is a network of connected VMC nodes distributed over the physical structure. The nodes have access to local sensors and transfer the flows of resource and successin to their children and parents. Since leaves and interior nodes play distinct roles, they might take different sensory information into account. For example, leaf nodes may sense the local intensity of light and temperature for producing successin while interior nodes may sense the tilting of or the mechanical stress on the module to adapt the rate of successin transfer accordingly (e.g., to add a preference for growing branches under less mechanical stress due to environmental and structural conditions).

4.2 Parameter setup

In the following set of experiments, two input sensory variables are implemented, I_{light} and I_{tilt}. The input variable I_{light} measures the local light and is used at the leaves, while I_{tilt} reads the local accelerometer (indicating the tilt of the branch) and is used at the interior nodes. The parameters for the experiments are chosen based on the understanding of the parameter effects obtained from the previous section and preliminary experiments. The parameters may vary according to the focus of each particular experiment and its conditions, e.g., light setting. The value of input variable I_{light} is the average of all four light sensors scaled to [0, 1]. Successin is produced at the leaves (Eq. 1) only based on the value of I_{light}. Therefore, $\omega_{light} = 1$ with no constant production rate (i.e., $\omega_c = 0$). Due to technical reasons[6] with respect to the implemented communication protocol, the successin values at all leaves are rescaled with a factor of 0.167. The accelerometer readings are also scaled to [0, 1] (where 1 means upright and 0 indicates upside-down) to obtain the input variable I_{tilt} which influences the transfer rate at interior nodes (Eq. 2). To compute the transfer rate, the input value is weighted by ρ_{tilt} and added to the constant transfer rate $\rho_c = 0.5$ (unless stated otherwise in the experiment). In most of the following experiments, the measured value of $I_{tilt} \simeq 0.99$ and $\rho_{tilt} = 0.5$; thus, the transfer rate is $\simeq 0.99$. The different cases are explained within the descriptions of the respective experiments. In most experiments, $\alpha = 0.9$ and $\beta_c = 2$ are chosen to allow fast adaptation and a medium competition, respectively. In all experiments, $R_{root} = 1$.

4.3 Growing structures with different competition intensities

In this experiment, two structures are grown in identical conditions with different values for the competition term, $\beta_c \in \{1, 2\}$. A light source is located at the top left of the structures. The experiment demonstrates the different behaviors of the structures in terms of growing toward light. The chosen threshold values for addition and deletion of nodes are $th_{add} = 0.25$ and $th_{del} = 0.2$, respectively. When several branches are ready to grow, i.e., when their resource is higher than the threshold, the user is free to choose the option they personally prefer. Figure 5 shows the growth[7] of the structure with $\beta_c = 2$. For every growth event, a new module is added to one of the leaf branches with resource higher than th_{add}. If several options are available, the user prefers the branch with the highest resource. Figure 6 shows the growth of the structure with $\beta_c = 1$. Because β_c cannot have any influence on the behavior of the first single module, we started the experiment with a second module already connected (step A in Fig. 5). The figures indicate the positive effect of the competition term on directing growth in brighter regions. With the high value for the competition term, the structure directly grows toward the light while it grows symmetrically (bushy) with a slight tendency to the brighter side when the competition term is low. Note that only for identical light conditions, the behaviors for the two values of the competition term are comparable. That means, for example, the small competition term ($\beta = 1$) in an environment with a different lighting conditions, may result in a structure which is more asymmetric than the structure shown in Fig. 6.

---

[6] The communication protocol used here limits the values in the interval [0, 1]. Since successin from different leaves is added together on its way to the root, we need to define a scaling factor according to a maximum value allowed for the number of leaves in a structure. In the following experiments we set the maximum value to 6 (a maximum of 6 leaves in the structure) and therefore the scaling factor is set to $1/6 = 0.167$. See Hofstadler et al. (2018) for more details on the communication protocol.

[7] A video of the growth experiment is available at https://youtu.be/-niKFhrXocI.
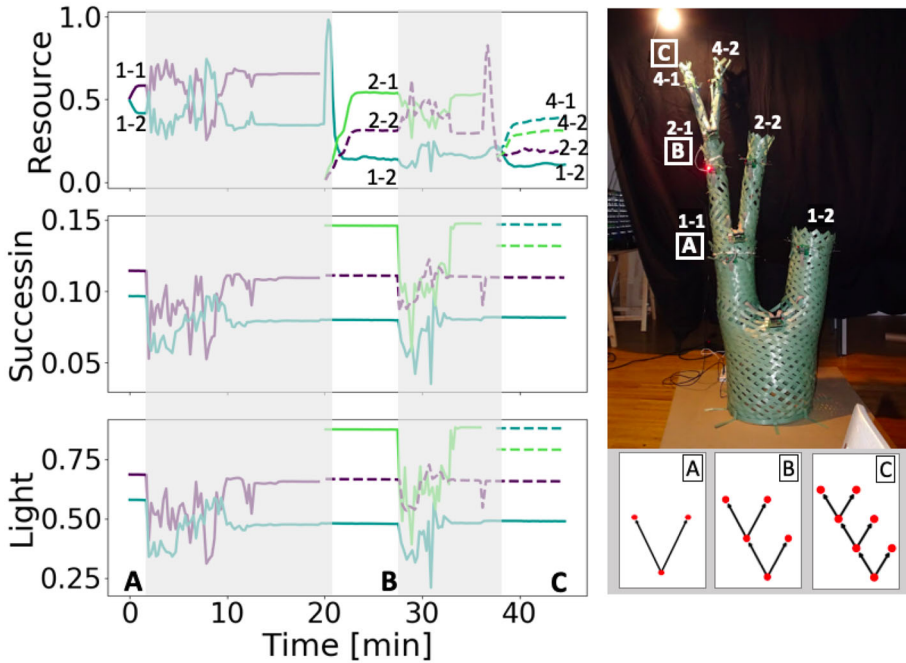
Fig. 5 Growth with $\beta_c = 2$. The plots on the left demonstrate the values of resource, successin, and the light input for selected nodes over the course of the growth. The final structure is depicted on the right. The A–C labels in the plots mark the steps right before the start of manual growth. In the photo of the final structure, the labels indicate the position of growth at each step. The shaded parts of the plots indicate the periods when growth was physically realized. The labels 1–1, 1–2, etc. mark the location of the selected nodes on the structure and their corresponding values (resource, successin, light) on the plots. The graphs on the bottom right depict the virtual VMC graphs running on the structure at each step of growth

4.4 Combined effect of transfer rate and competition intensity

In this experiment the combined effect of transfer rate and competition intensity is investigated. The final structure from Fig. 5 is used as presented in Fig. 7. Here, instead of the directional light source as in Fig. 5 (located top left of the structure), the experiments are performed under ambient room light. The lights received by the different leaves differ from each other due to reflections and shadows in the environment. However, the variation is much lower than in the experiment shown in Fig. 5. The constant transfer and competition parameters are $\rho_c \in \{0.25, 0.5\}$ and $\beta_c \in \{1, 2\}$. Considering that $\rho_{\text{tilt}} = 0.5$ and $I_{\text{tilt}} \simeq 0.99$, then $\rho = \text{TRANSFER} \in \{0.74, 0.99\}$.

Table 2 shows the resource and light values of all leaves, with the maximum resource value of each setup represented in bold and the maximum light values represented in italic fonts. As shown in the table, there are only small changes in the light values of each leaf between the different setups. In all setups, leaf 2–2 receives the most light. The leaves 1–2 and 4–1 follow, with 1–2 being slightly higher. Leaf 4–2 receives the least amount of light. With $\beta_c = 1$ and $\rho = 0.99$, ordering the leaves based on their resource values directly reflects the order of their light values: 2–2, 1–2, 4–1, 4–2. With the same $\beta_c = 1$ and lower transfer rate $\rho = 0.74$, the order changes in favor of the shorter branch, preferring 1–2 over the 2–2. For $\beta_c = 2$, $\rho = 0.99$, the combination conditions act in favor of the longer branches. In this case both 4–1
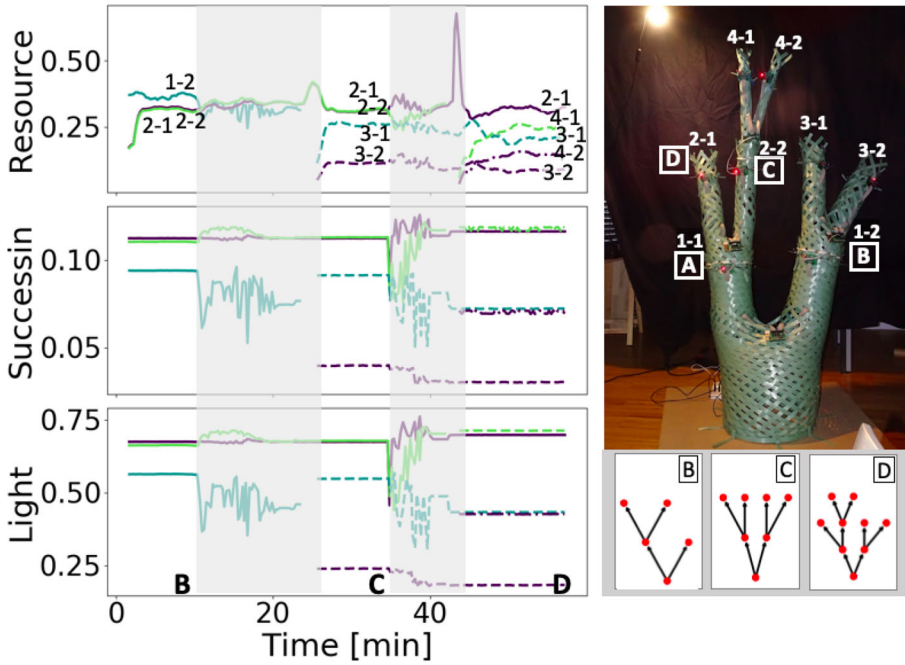
$\underline{\textcircled{\tiny 2}}$ Springer

Fig. 6 Growth with $\beta_c = 1$. The plots on the left demonstrate the values of resource, successin, and the light input for selected nodes over the course of the growth. The final structure is depicted on the right. The A–D labels in the plots mark the steps right before the start of manual growth. In the photo of the final structure, the labels indicate the position of growth at each step. The shaded parts of the plots indicate the periods when growth was physically realized. The labels 1–1, 1–2, etc. mark the location of the selected nodes on the structure and their corresponding values (resource, successin, light) on the plots. The graphs on the bottom right depict the virtual VMC graphs running on the structure at each step of growth

Fig. 7 The structure that is used to show the combined effect of transfer rate and competition intensity. The experiments are performed under ambient room light
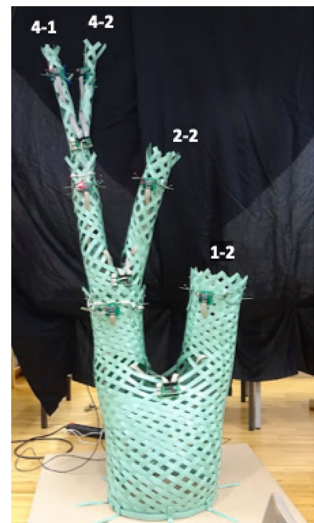
ρ	β_c	State var.	1–2	2–2	4–1	4–2
0.99	1.0	Resource	0.252	**0.268**	0.247	0.219
		Light	0.809	*0.857*	0.793	0.702
0.74	1.0	Resource	**0.358**	0.279	0.189	0.168
		Light	0.806	*0.854*	0.791	0.699
0.99	2.0	Resource	0.112	0.227	**0.364**	0.287
		Light	0.806	*0.849*	0.787	0.698
0.74	2.0	Resource	0.231	**0.289**	0.263	0.205
		Light	0.804	*0.853*	0.791	0.698

Table 2 Combined effect of competition and transfer rates

and 4–2 as longest branches get more resource than 2–2 and 1–2, while the 4–1 is preferred due to a higher light value. For $\beta_c = 2$, $\rho = 0.74$, the combination is more complicated. Leaf 2–2 that receives the most light and has a medium path length to the root, gets the most resource. But the next choice is the 4–1 with a long path to the root, even with slightly less light compared to leaf 1–2. Overall, the experiment indicates that the lower transfer rate creates a tendency for shorter paths, and a higher competition intensity creates a tendency for further growth of larger branches. This is in line with the discussion in the previous section.

4.5 Regulating growth in particular branches by using a sensor-dependent transfer rate

This experiment demonstrates the effect of the sensor-dependent transfer rate (Fig. 8). The experiment is performed in ambient room light. After the first few minutes of the experiment with the intact structure, we bend the leftmost branch such that I_{tilt} decreases considerably. Figure 8 shows the variable values throughout the experiment. It shows that bending a branch leads to small values of I_{tilt}, decreases the transfer rate in the associated interior node and results in a lower share of the resource for that branch which may eventually restrict its growth.

4.6 The effect of the adaptation rate

In this experiment, we investigate the effect of the adaptation rate on the speed of resource dynamics. A directional light source is placed at the top left of the structure as demonstrated in Fig. 9 (top). To investigate the response time of the system to the changes in the environmental input, an experimenter casts a shadow on the leftmost branch of the structure at various intervals of time. The experiment is repeated with two different values for the adaptation rate $\alpha \in \{0.1, 0.9\}$. We observe the light intensity as perceived by the sensors, successin production, and resource values of all the three leaves of the structure. Figure 9 (bottom) demonstrates the variable values during the experiment for both values of α. The figure shows gradual changes in the resource level with the low value of $\alpha = 0.1$, reflecting a slow change in the vessels—a memory of the system stored across the structure. On the other hand, with $\alpha = 0.9$, resource values respond very quickly to the changes in the sensor inputs, reflecting a fast change in the thickness of vessels. Depending on the application, fast or slow response times can be desirable. For example, the slow dynamics of vessels with $\alpha = 0.1$ result in a delayed response to changes, filtering out the variations in light as environmental noise. As a result, the structure continually prefers the leftmost branch. On the other hand,
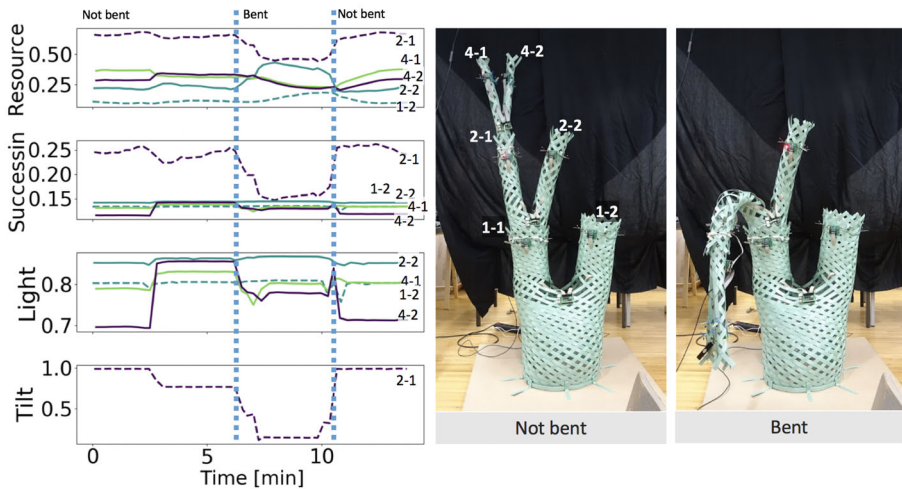
Fig. 8 Values of resource, successin, input light variable (sensed at the leaves), and the tilt variable (sensed at the interior node) in the course of the experiment demonstrating the effects of a sensor-dependent (tilt-dependent) transfer rate. The structure is intact at first, then the left branch is bent for a period of time (indicated in the plots and depicted on the right), and then released again. The tilt value is shown only for the interior node 2–1 which is the node that senses the bending. The light input values are shown for the leaves. The resource and successin values are shown for both the leaves and the interior node 2–1

in the experiment with $\alpha = 0.9$, fast response to the changes leads to the preference switching between two branches (i.e., the leftmost and the middle).

4.7 Adaptation of shape to changes in the environment

Figure 10 shows an example of an adaptation of shape to changes in the environment. The value of $\beta_c = 1$ and both addition and deletion are possible. The experiment is performed in two stages. In the first stage, a weak light is switched on at the top right of the structure. The structure starts from an initial module and grows toward the light (steps A–C in Fig. 10). In the second stage, a stronger light is added to the environment at the top left of the structure (step D in the figure). The structure reacts to the change by growing new modules at the left side while losing the ones at the right (steps E–H). The final structure's shape is the same as the one at the end of the first stage but reflected over the y-axis. Figure 10 shows the structure's shape at each step of the growth, along with the resource, successin, and light values at every leaf.

5 Numerical investigation of parameter effects

In this section, we investigate a broader range of parameter setups with larger VMC graphs in several simulation experiments. In this section, we investigate a broader range of parameter setups with larger VMC graphs in simulation. The intention here is not to repeat the physical experiments with large numbers, but to study other intrinsic morphological aspects of VMC and their dynamics. More specifically, here we study the internal tendency of the VMC structures toward asymmetry of the shape and dynamics of the morphology (i.e., growth and retraction) in the absence of any environmental asymmetry (e.g., any variation or gra-
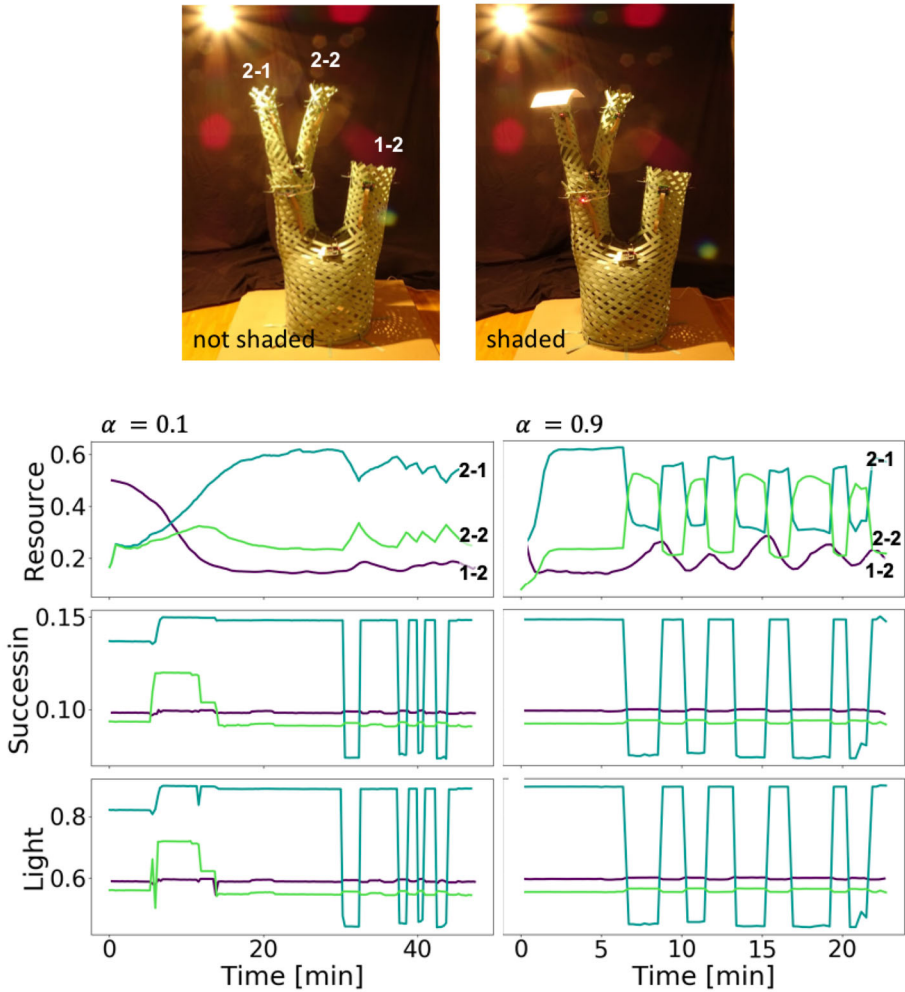
Fig. 9 Top: the structure in both shaded and unshaded conditions. Bottom: the variables over the course of the experiment with periods of shaded and unshaded conditions with two different values of adaptation rate α. The results show a slow reaction to the change in lighting condition (shading/unshading) for small α and a quick change for the large α (note the different scaling of the x-axis of the diagrams)

dient existing in the environment) or structural information. For that, no external effects are implemented, i.e., no sensory information or physical interactions either inside the structure or between the structure and the environment. Therefore, the dynamics and behaviors are merely the results of internal interactions and dynamics via the vessel system. We limit the study to a setup with one root node and two children for every node. The simulation starts with the root node and its two children: one child positioned at the left side and the other at the right side of the root. None of the nodes of this initial structure are removable during the experiment. Fig. 11 shows two schematic example structures with the same number of nodes and different shapes. In the following, we present the set of experiments to investigate the effects of parameterization on some intrinsic morphological behaviors of the VMC. Since there is no environmental information, we set all the sensor-dependent parameters to zero.
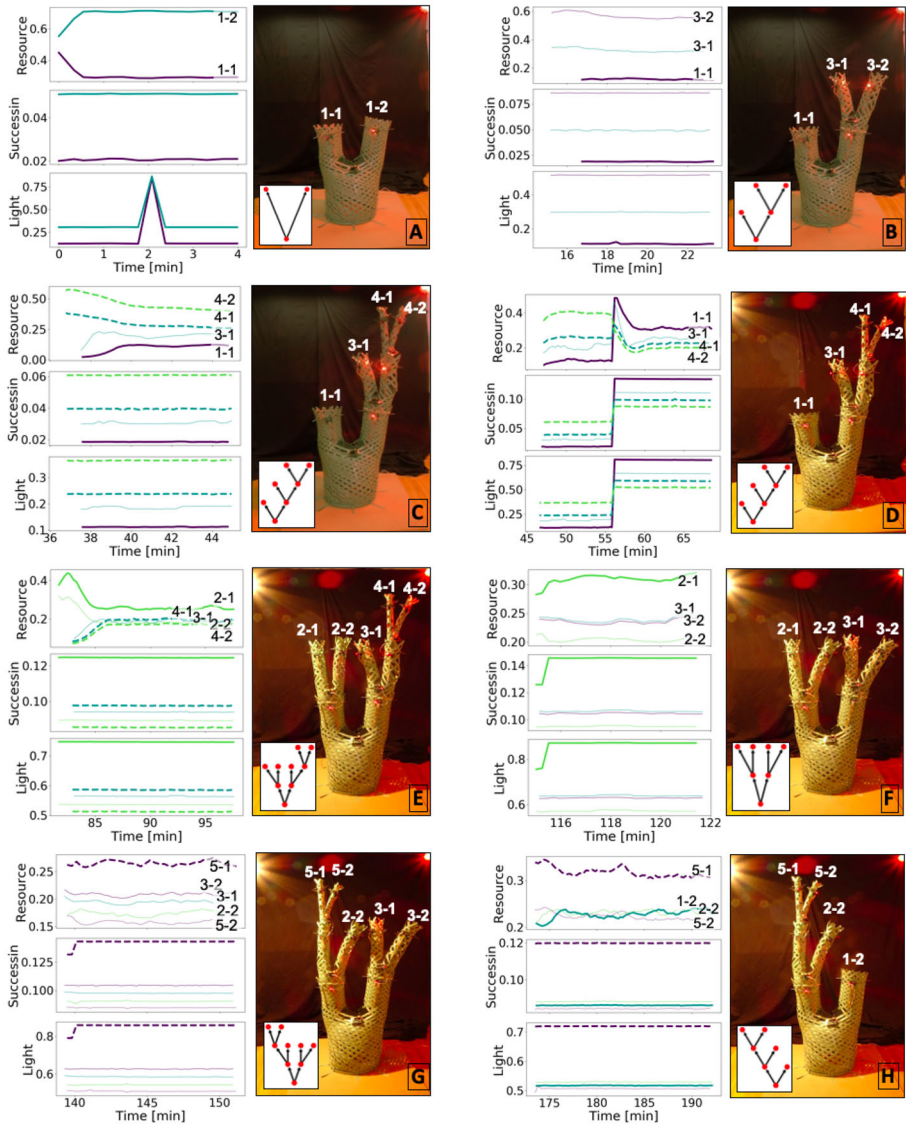
Fig. 10 The shape of the structure adapts to changes in the environmental inputs. In the first stage (**a–c**) only a weak light is switched on at the top right. After the growth of the structure toward the light, a stronger light is also switched on at the top left (**d**). The shape of the structure changes accordingly (**e–h**). Note that the light value of each branch is the average of all the four sensors positioned around the branch and the orientation of the sensors and shadows contribute to the perceived values

5.1 Morphological aspects: asymmetry and dynamicity

The two children of the root make the two main branches of the structure. We measure the asymmetry of the grown structures concerning these two main branches. Here, we define the asymmetry at the end of a run as the absolute difference between the proportion of nodes at the two main branches, as follows:
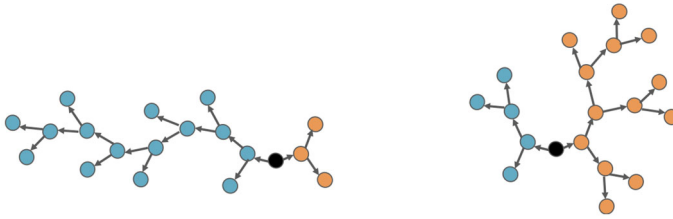
Fig. 11 A schematic of two example structures with the same number of nodes. The nodes at the left main branch are indicated in blue and the nodes at the right main branch are indicated in orange

Table 3 List of parameters and their values

Parameter	Value
α	0.1, 0.5, 0.9
β	0, 0.5, 1.0, 2.0, 10.0
ρ	0.25, 0.5, 0.8, 1.0
ω	0, 0.1, 1.0
c	1
R_{root}	20

$$\text{asymmetry} = \frac{|N_{\text{L}} - N_{\text{R}}|}{N_{\text{TOTAL}}} \qquad (19)$$

where N_{L} and N_{R} are the number of nodes at the left and right side of the structure, respectively, and N_{TOTAL} represents the structure's size which is the total number of nodes excluding the root.

In addition to the asymmetry that concerns the final morphology, we also use a measure of dynamics during growth. We define dynamicity as the ratio between the number of deleted nodes during growth and the final size of the structure:

$$\text{dynamicity} = \frac{D}{N_{\text{TOTAL}}} \qquad (20)$$

where D is the number of nodes that are deleted during the course of the experiment.

A set of simulation runs with different parameterizations is performed. Every run starts with the root node and its immediate children. For a stop condition of a run, we keep track of the structure's size and always record the maximum it has ever reached up to now. The stop occurs 50 timesteps after the last increase in the recorded value. Reaching this stop condition in a limited time is guaranteed by setting the consumption term of the nodes (c) to a positive value that constrains the size of the structure. Since all the sensor-dependent parameters are zero, in the following we, respectively, use β, ρ, and ω to indicate β_{c}, ρ_{c}, and ω_{c}. Note that without the sensory information, the successin produced in all the leaves is equal.

Table 3 shows the different parameter values used in the simulations. For each parameterization, we perform 25 independent repetitions. Here, if all the children of a node have a resource value below 1 ($\text{th}_{\text{del}} = 1$), they will be deleted altogether with a high probability (95%). The probability of adding children to a leaf i is proportional to its share of the resource (R_i/R_{root}). To prevent several leaves from growing at the same time, we keep the candidate leaves in a pool. In each timestep, only one of them is selected randomly to realize the growth.

Figure 12 shows the asymmetry and the dynamicity of the different setups and the corresponding structures' sizes. The bars represent the values averaged over all repetitions, and
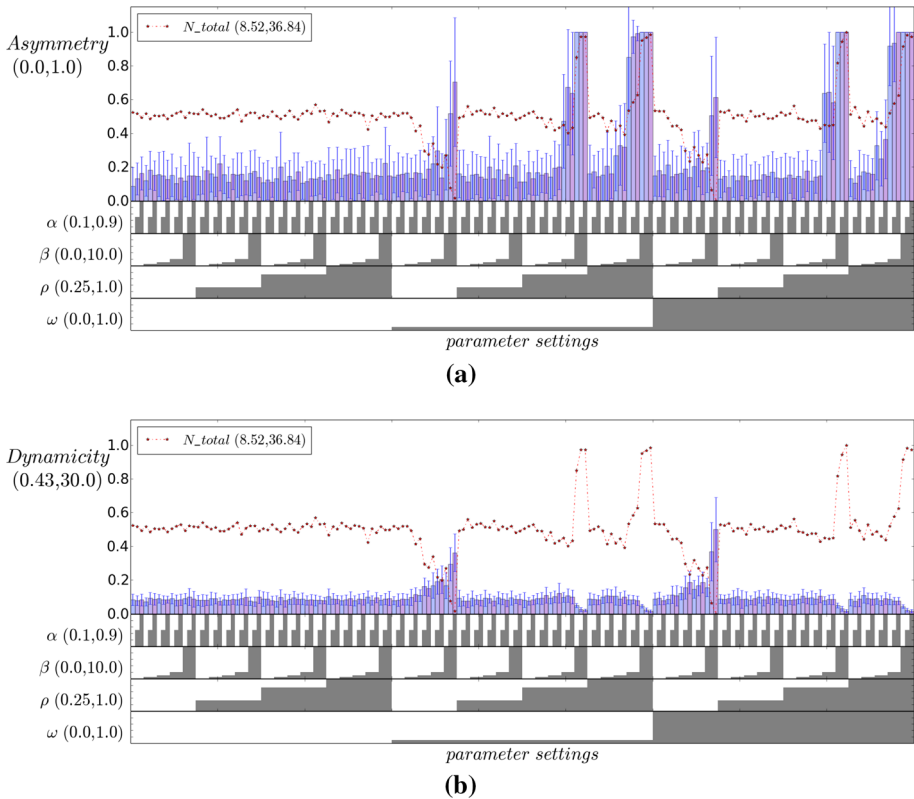
(a)

(b)

Fig. 12 Asymmetry and dynamicity of VMC structures with different parameterizations. The colored bars (top part) represent the values averaged over all the repetitions and the whiskers represent the standard deviations. The red dots represent the number of nodes in the structure at the end of each run. The gray bars (bottom part) indicate the values of each parameter (Color figure online)

the whiskers represent the standard deviations. As seen in the figure, $\omega = 0$ leads to relatively symmetric structures with a medium nodes' number and low dynamicity. The reason is that without any input (sensor) or constant production rate, no successin is produced. Therefore, independent of other parameters, there is no difference between the thickness of vessels, leading to an equal distribution of the resource. The minimal asymmetry seen in the figure is only due to the transient effect of the randomness in the selection of leaves for growth.

Looking at the setups with $\beta \leq 1$, the structures are symmetric. This is inline with the results of the analysis in Sect. 3.3, implying that $\beta \leq 1$ is a sufficient (but not necessary) condition for the tendency toward growing symmetrically (when all other conditions are equal).

For values $\omega > 0$, $\rho > 0.5$, $\beta > 1$, the structures are asymmetric with low dynamicity. With the high value of $\beta = 10$, dynamicity is minimal, reflecting the low amount of deletion during the growth process.

For values of $\rho \leq 0.5 = \frac{1}{n}$ (where $n = 2$ is the number of children of a node), the structures are symmetric except for the setup with $\omega > 0$, $\rho = 0.25$, $\beta = 10$. This exception seems to be deviating from the theoretical analysis[8] in Sect. 3.3, which stated that the necessary

---

[8] Note that the analysis assumed convergence of values which is not necessarily the case for all setups.

condition for a tendency toward asymmetry is $\rho > \frac{1}{n}$ and therefore predicting symmetry for $\rho < \frac{1}{n}$. The same effect (high asymmetry and deviation from the theory) can also be seen for other values of $\rho < \frac{1}{n}$ (an example will be shown below). The reason for this unpredicted behavior is the delay in the update of the values within the structure. It is more clear when looking at the extreme case of $\rho = 0$. In this case, no successin passes from one level to the next. Thus all connections get a successin of zero, except the ones behind the leaves. Hence, as soon as a leaf becomes an interior node, the connection's thickness decays. Now, consider a growth scenario starting from the initial structure (the root and its two children). In the beginning, the two leaves get the same share of the resource, thus equal chances for growth. With the first growth event (at either branch), the connection weight of the grown node starts to decay toward zero (with the rate α), and its share of the resource follows. However, the node continues to distributing its resources among its children, and that might be enough to allow them to grow as well. For a while, the grown branch keeps growing as it has more leaves with enough resources and thus higher chances for further growth. Meanwhile, the resources increase significantly at the non-grown side as the first connection to the grown side reaches zero. Therefore, the single leaf starts growing, which again goes through the same process of connection decay and resource distribution among children as they emerge. In parallel, the former large branch loses its nodes due to a shortage of resources at the leaves. The deletion continues until there are no leaves left at that branch, except a child of the root. This node is a leaf attached to the root, thus a large successin and connection thickness, pulling the resource and growth at that side. This way, the fluctuating asymmetry between the two main branches continues. The fluctuation can be recognized by looking at the measure of dynamicity and the size of the structure. Figure 12b shows comparatively large dynamicity values and fewer nodes (smaller structures) for all setups with $\omega > 0$, $\rho = 0.25$, $\beta > 1$. Recall that the dynamicity reflects the ratio between the deletion rate during the growth process and the structure's size.

Figure 13 shows the asymmetry, dynamicity, and the number of nodes for a parameter sweep experiment on the values of ρ. The experiment uses a setup with $\omega = 0.1$, $\beta = 10$, and $\alpha = 0.9$. As seen in the figure, around the critical value of $\rho = 0.5 = \frac{1}{n}$ (where $n = 2$ is the number of children of a node), the behavior changes from high dynamicity and small structures (few nodes) to large and stable structures. The measured asymmetry increases both above and below the critical value. Above that, the asymmetry and the number of nodes grows, but the dynamicity declines. That means, if $\rho > \frac{1}{n}$, large stable structures grow increasingly asymmetric for higher values of ρ. Below the critical value ($\rho < \frac{1}{n}$), the high asymmetry, the tiny number of nodes, and high dynamicity indicate fluctuations of small unstable structures with a few nodes repeatedly growing and disappearing again on one side or the other.

5.2 Decision making performance of the collective system

The addition and deletion events in this section follow a probabilistic implementation as described before. Due to the probabilistic nature, every growth trajectory shows fluctuations in the number of nodes of the two sides of the structure. Likewise, the resources assigned to each side change. The assignment of more resources to one side is called a *decision* of the structure for choosing that side. Figure 14 shows examples of decisions represented as the fraction of the resource on the left side of the structure. The fraction is calculated as $f_L = R_L/(R_L + R_R)$, where R_L and R_R are the resource at the left and the right side, respectively.

As expected from the previous section, the behaviors for the various settings demonstrated in Fig. 14 are different. For example, Fig. 14a shows unstable decisions with a large amplitude of quick variations in the amount of the resource allocated to each side. With the setting used
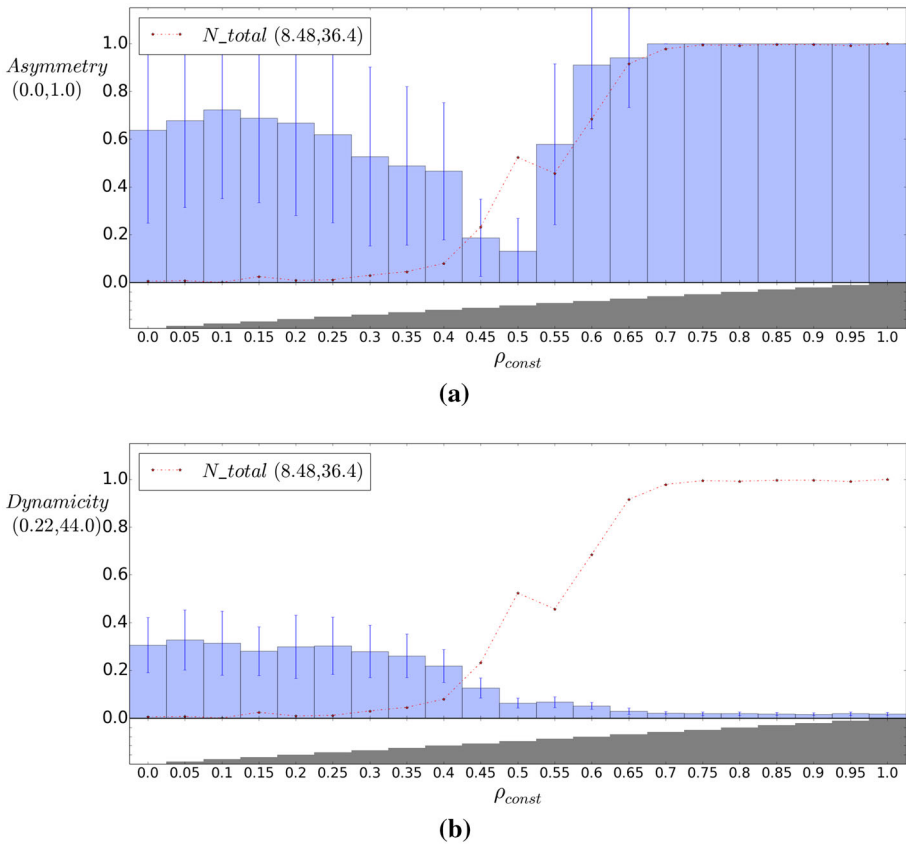
(a)

(b)

Fig. 13 Asymmetry, dynamicity, and number of nodes for VMC structures with different transfer rates (ρ) in setups with $\omega = 0.1, \beta = 10, \alpha = 0.9$

in Fig. 14b, the decision fluctuates slowly and with a small amplitude. Thus the resource allocated to the sides does not converge during the experiment. In Fig. 14c, the structure quickly chooses one side to grow by assigning most of the resource to it from the early steps. The example of Fig. 14d shows some fluctuations in the amount of the resource and a final convergence to one of the two sides.

The presented behaviors are a result of the competition for the limited resource provided at the root, i.e., R_{root}. In the following, we investigate the influence of R_{root} on the performance of the decision making of the structures. For that, we used the parameter settings of the experiment from Fig. 14d, which exhibits some dynamics with a period of fluctuations and eventual convergence to a decision. We define *performance* as the difference between the resources at the two sides, after a fixed period:

$$\text{Performance} = |R_L - R_R|/(R_L + R_R) \tag{21}$$

where R_L and R_R are the amount of resource allocated, respectively, to the left and the right sides of the structure after 250 timesteps. The *performance* is measured for a set of different values of R_{root}. We repeat the measurement in every setting for 9000 independent runs. Figure 15 shows the median performance of the tested R_{root} values. The inset image

(a) $\alpha = 0.9, \beta = 2, \rho = 0.25, \omega = 0.1$

(b) $\alpha = 0.9, \beta = 1, \rho = 0.8, \omega = 0.1$

(c) $\alpha = 0.9, \beta = 10, \rho = 0.8, \omega = 0.1$

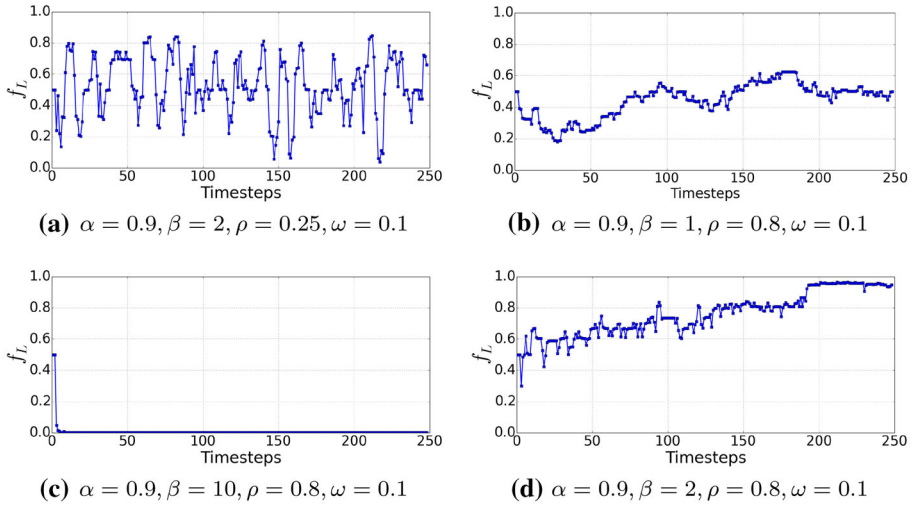**(d)** $\alpha = 0.9, \beta = 2, \rho = 0.8, \omega = 0.1$

Fig. 14 Example trajectories of $f_L = R_L/(R_L + R_R)$, the fraction of resource assigned to the left side of the structure for different parameter settings. In all examples $R_{root} = 20$ and all the sensor-dependent parameters are set to zero
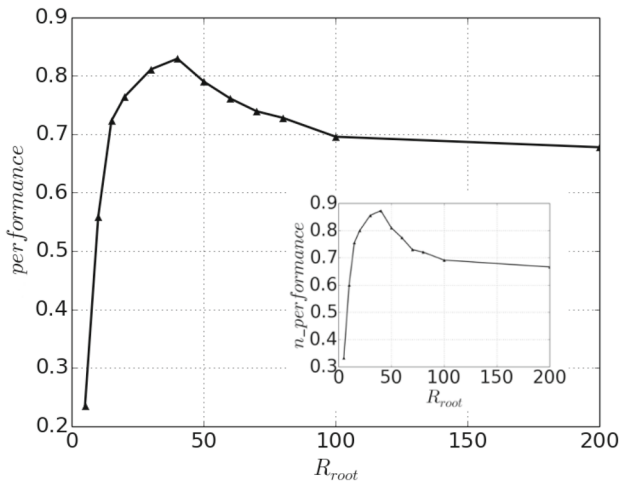

Fig. 15 Performance of the decision for one side of the structure with different values of R_{root}. The triangular dots represent median performance of 9000 independent runs for each setting. All the sensor-dependent parameters are set to zero. The inset image shows the performance computed based on the number of nodes at the end of the run instead of the resource values

shows the performance computed based on the number of nodes at the end of the run instead of the resource values (i.e., the asymmetry measure $|N_L - N_R|/N_{TOTAL}$)).

In Fig. 15 we see very poor performances for very low values of R_{root}. The performance moves up with the increase in R_{root}, and after an optimum value for R_{root} (~ 40 in this case), it drops again and then stabilizes (relatively high comparing to the performance of very low values of R_{root}). The shape of the curve is similar to the generic diagram of system performance over system size for multi-robot systems discussed in Hamann (2018a). The available
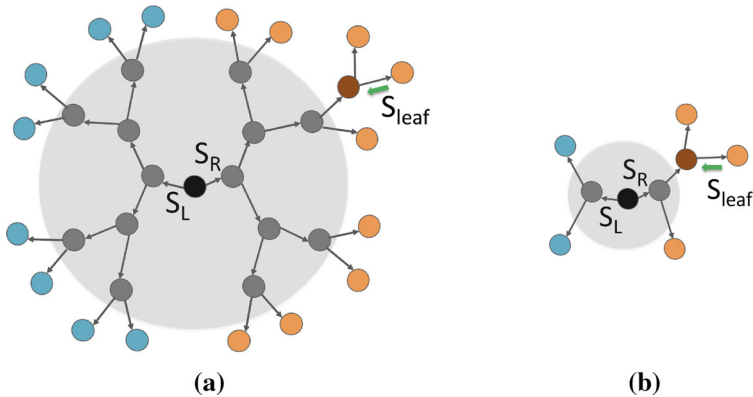
Fig. 16 Two example systems with larger (**a**) and smaller (**b**) system sizes. The leaves of the left and right sides are visualized with blue and orange colors, respectively. All leaves produce the same amount of successin, S_{leaf}. A recently grown node is depicted by dark red. The amount of successin reaching the root from the left and the right side are represented by S_L and S_R. The change in successin reaching the root due to the growth of a node is larger in a small system compared to a large system (Color figure online)

resource (R_{root}) is representative of the system size as it is nearly linearly proportional to the final number of nodes in the structure. The reason for this proportionality is that every non-leaf node holds a constant fraction of the resource (the consumption term).[9] The shape of the performance curve is similar to multi-robot systems with low interference between the robots, for example, due to a body-less (point-like) simulation of robots (Hamann 2018a). That is consistent with the fact that in the current system, we have not implemented any physical effects that could cause physical interactions and potentially lead to interference between the nodes.

As discussed in Sect. 3, the preconditions for a tendency toward asymmetric growth in VMC is $\beta > 1$ and $\rho > \frac{1}{n}$, where n is the number of children in every growth event. Both conditions are satisfied in the settings that are used here with $n = 2$, $\rho = 0.8$, $\beta = 2$. Such a tendency to asymmetry is the positive feedback effect of growth and means further growth at branches with more nodes.

Although the positive feedback leads to reinforcement of asymmetries and higher performance, it has a smaller effect in larger systems compared to smaller ones. The following example makes it more clear by comparing two systems of the same symmetric conditions but different sizes. (Figure 16 illustrates two example systems.) Let G be a perfect binary tree of depth r. After a growth event at the right branch and assuming an identical successin production of S_{leaf} at all the leaves, the successins at the main left and right branches are: $S_L = (2^{r-1})\rho^r S_{\text{leaf}}$, $S_R = (2^{r-1} - 1 + 2\rho)\rho^r S_{\text{leaf}}$. Hence the proportional successin difference between the left and right branches is $(S_R - S_L)/(S_R + S_L) = (2\rho - 1)/(2^r - 1 + 2\rho)$. The r is larger in a bigger system, and therefore, such a system has a lower proportional difference. In other words, the effect of a change diminishes as a result of the long path to the root. In a small system, a change has a higher effect on resource distribution in favor of the larger branch. That leads to a higher positive feedback effect and amplification of growth and facilitates decision making.

The decrease in the positive effect of growth when increasing the system size can explain the lower performance of the larger systems demonstrated in Fig. 15. However, where the

---

[9] The number of non-leaves is linearly proportional to the number of leaves in such a graph, e.g., in a 2-branch tree graph (as used here) the number of non-leaves equals the number of leaves minus one.

system is too small (very small R_{root}), the robustness of the positive feedback effect is reduced. That is because the amplification effect has two sides: a change in the resource distribution and growth in the system can be either due to positive feedbacks following the previous growth events or due to random fluctuations. Random fluctuations are easily amplified at first and lead to a difference between two sides of the system. However, when the resource is too little, the amplification of the first events cannot continue long enough to produce many new leaves at the majority side. The reason is that after a few steps, the leaves of the majority branch get too little resource that limits their chance of growth (negative feedback). That makes their conditions similar to the leaves of the other branch. Thus the next growth events rely mainly on random fluctuations. As mentioned above, changes have a greater impact on smaller systems. Besides, with tiny resources, the early termination of growth in the majority branch, the difference between the leave numbers (i.e., the options for random growth) of the two branches never gets large. Therefore, when growth occurs at the minority side due to a random event, it is hard to be compensated by the majority side. Thus the change at the minority side might be reinforced and make it the new majority, which is again unstable. It can explain the poor performances of the tiny systems, seen in Fig. 15.

In short, one can see the performance as the effectiveness of the positive feedback on the asymmetry that leads to a majority decision. For high values of R_{root}, the negative contribution of the length of the main branch reduces the performance, whereas, for very low values of R_{root}, the performance is low because the negative feedback (limitation of resource) cancels out the positive feedback in early stages and therefore the random fluctuations are the main contributors to the dynamics. The performance peak is where the two effects balance each other.

6 Discussion

We performed the theoretical analysis of VMC in the absence of any environmental effects. The results demonstrated an intrinsic tendency of the VMC for shorter paths. However, they also showed that with an appropriate parameterization (high transfer rate ρ and competition intensity β), a tendency toward larger branches and asymmetric growth is also possible. These tendencies, in combination with environmental inputs, determine the morphological behaviors and dynamics of the structure. For example, they may determine how the structure grows in a multimodal environment and how it behaves for local and global optima. The primary effect of environmental inputs is their influence on the production of successin in the leaves, which in turn influences the growth. As a result, the structure grows further in regions with more favorable environmental inputs. However, the behavior of the structure in terms of exploitation vs. exploration depends on the parameterizations. The parameters determine the structure's tendency to explore various options (toward symmetry), to stick to older decisions, or to exploit the current best choices. The exploitation of the current best options means growing further in the local optima of the environment, i.e., growing branches that are currently in favorable regions. A tendency toward sticking to older decisions (historical choices) is the preference for following decisions that are made in the past, i.e., larger branches. A branch can be chosen to grow because it is large, even if it is not in a favorable region anymore. The actual decision of the structure depends on both the parameters and the gradients of inputs in the environment. We present an example of such tendencies in a physical experiment in Sect. 4.4, where we test a set of different parameters. With $\beta = 1$, $\rho = 0.99$, the structure clearly exploits the current environment, preferring the leaf

with the highest light value. With $\beta = 2$, $\rho = 0.99$, the structure prefers to stick to old decisions by choosing the two longest branches, with a preference for the one receiving more light. In the light conditions of the given environment, with $\beta = 1$, $\rho = 0.74$, the structure prefers the shortest branch. With $\beta = 2$, $\rho = 0.74$, however, the first choice in these conditions is the branch with the highest amount of light, which is a medium-sized branch. The second choice is a longer branch with slightly less light than the third choice, showing a tendency toward old decisions (preference for longer branches) rather than picking the currently better options. An example of such a tendency to stick to taken decisions, known as *apical dominance*, exists in plant morphogenesis, where a growing tip suppresses the outgrowth of new branches behind it (also) by consuming the necessary resources (Sachs 2006; Kebrom 2017). Further investigation of parameters, in particular, the sensor-dependent parameters, will provide more information about the behaviors where different tendencies are combined. Moreover, future investigations are required to demonstrate the adaptivity of the structures in response to environmental changes and the reaction time of adaptation.

In the simulation studies in Sect. 5.1, we demonstrated the effects of different parameterizations in the dynamical and morphological behaviors of the structures. An interesting point is the effect of the transfer rate ρ on the structure's dynamic behavior. Low values of $\rho < \frac{1}{n}$ (where n is the number of children of a node) lead to unstable small structures where a small number of nodes appear and disappear quickly, causing large fluctuations in small structures. On the other hand, high values of $\rho > \frac{1}{n}$ lead to stable and large structures. The reason for this difference in behaviors lies in the fact that with $\rho < \frac{1}{n}$, the transfer of information (successin) from children to parents is too inefficient. For example, consider two nodes A and B with the same parent P, where A is a leaf and B has n child leaves. Let's assume that all the leaves produce the same amount of successin, S_{leaf}. The successin transferred from A to P is S_{leaf}, while the successin transferred from B to P is $\rho n S_{\text{leaf}} < S_{\text{leaf}}$ (with $\rho < \frac{1}{n}$). That prevents the vessel system, i.e., the memory of the system stored spatially, from reflecting the structure's shape and status. That means the distribution process is uninformed about the current structure and therefore cannot build upon the previous steps which leads to instability. Once the transfer rate allows a monotonic correlation between the structure's status (e.g., shape) and the vessel system, i.e., $\rho > \frac{1}{n}$, distribution and growth can be performed accordingly. This is a situation that leads to stability. The change from instability to stability and the explosion of size makes ρ an interesting parameter with a critical value at $\rho = \frac{1}{n}$.

As discussed in the previous section, the diagram of decision making performance against the common resource (Fig. 15) displays similarities with the generic diagram of system performance over system size in multi-robot systems (Hamann 2018a). In general, one can draw an analogy between the collective process of growth in a VMC structure and a collective decision making process in a multi-robot system or a swarm of agents. As an example, consider a multi-robot decision making scenario where the robots are confronted with two choices. In the beginning, the individual robots choose one of the two possibilities with equal probability because any potential effect of interactions has not yet appeared. With the robots being the system's limited resource, the resource is initially distributed more or less equally between the two options. Over time, the distribution may change due to fluctuations and interactions between the robots and may drive the system to make a collective decision choosing one of the options over the other. The robots in this scenario are both the distributed limited resource and the active agents that carry out the distribution via a collective dynamic process. On the other hand, in the VMC system, the concept of resources distribution is more explicit. In an example VMC, the growing system distributes a limited resource between its two sides (left/right branches). The resource is materialized as the nodes that form the structure—recall that a constant amount of resource (the consumption term) is kept

Fig. 17 Feedback loops for the resource stored on a path or branch
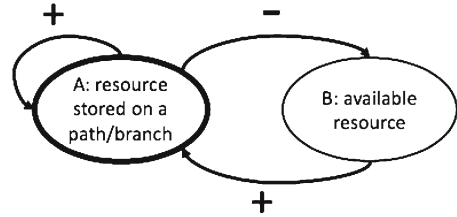
(consumed) within every non-leaf node, making the nodes representatives for that amount of resource; and a leaf node may trigger the growth of new nodes or its own removal, depending on the amount of resource it holds. In other words, the nodes act both as the representatives of the resource and the active agents carrying out the process of growth and distribution. Similar to the robotic scenario, the system begins with an equal resource distribution among the two options. Over time and via the system's fluctuations and interactions among the competing nodes, the distribution may vary and eventually reach a state where most of the resource is allocated to one side of the system for a long time.

Being inspired by plant morphogenesis, VMC acts on the branching of structures consisting of addable and removable components. It implements exploration of the environment as well as the reinforcement of most favorable branches while losing the least favorable ones. These concepts are shared with self-organized path formation by swarms of mobile agents. As an example, consider the pheromone trails connecting the nest of ants to patches of food (Detrain and Deneubourg 2006; Perna et al. 2012), which has inspired many researchers of artificial life and swarm robotics over the last years (e.g., Campo et al. 2010; Dorigo et al. 1996; Payton et al. 2001; Sperati et al. 2011). Initially, the individual scout ants that have found a food source lay pheromone in their randomly chosen path to the nest. The pheromone acts as a volatile memory that is stored spatially in the environment. It is perceived by other ants and guides them to the food source. The other ants reaching the food, in turn, lay pheromone on their way back to the nest, generating positive feedback leading to reinforcement of the shortest paths between the nest and the food sources. The role of the mobile agents (e.g., ants) in path formation is fulfilled in VMC by the flows passing through the connection paths that are imposed by the nodes of the directed graph. The positive feedback generated by the reinforcement of favorable paths for ants is similar to the positive feedback generated by the flows of successin in favorable branches of a VMC system. In both systems, the positive feedback collectively building up the paths is counteracted and stabilized by the negative feedback (Sumpter 2006). If the food source at the end of a path is limited, it can act as a negative feedback causing the ants to leave the path and form new ones. Another negative feedback more interesting here is the limitation of the number of ants as the limited resource for the structure of the paths. It is similar to the limited resource distributed among the different branches in the VMC. To make the role of the resource in the feedback loops more clear, Fig. 17 illustrates two variables that influence each other: (A) the resource stored on a path or branch contributing to the thickness of its segment (the path or branch); (B) the available resource that is not yet settled. The positive feedback is a direct effect of A on itself, but the negative feedback of A goes through B, i.e., the "available resource," as shown in Fig. 17. The positive feedback in the path formation of ants is influenced negatively by the volatility of the pheromones. In VMC, the positive feedback effect decreases by the negative contribution of the branches' length due to the transfer rate $\rho < 1$ (as discussed in the previous section).

In this paper, we implemented the VMC with a single root for each graph and in tree-like structures. However, the algorithm allows the implementation of several roots and multi-input

nodes (i.e., nodes with several incoming connections). The only restriction is to avoid directed cycles in the graph. If the graph contains several roots, each is an independent starting point for the resource. The resource provided by the roots may differ from one another. Their value, whether in a multi- or single-root structure, can be either constant or variable. A variable one may reflect a dynamic environmental parameter (e.g., the quality of ground) or a function of internal qualities, e.g., the amount of successin that reaches the root. Variable resources allow for more complex scenarios, i.e., structures growing in crowded areas receive less resource at their roots because they share an environmental source. Another interesting topic to explore is to consider non-tree-like structures. For example, VMC can grow a structure starting from one or several roots. During the process of growth, nodes that are very close to each other can merge. A similar process is possible in some plants where a growing tip can fuse into an existing branch (Slater 2018). A multi-input node receives the resource from all of its parents. Various strategies can be followed regarding the successin distribution among multiple parents, e.g., the successin can be equally divided or divided as a function of the vessel thickness or the received resource. Future investigations will determine the properties of each strategy.

Here, in the simulation studies, we implemented the VMC with no external interactions between the nodes, i.e., the only interactions occur via the vessel system. In general, however, VMC can be embodied in the structures that allow external (e.g., physical) interaction of nodes. For example, nodes can hinder the growth of nearby leaves by acting as an obstacle or casting a shadow on the lower levels. In a physical implementation, the growth of new nodes may increase the weight imposed on the lower branches. It may affect the parents via sensors or bending under pressure and repositioning of children. Despite the deterministic implementation of the algorithm, fluctuations in the environment, electronics, and humans may also contribute to the variations and stochasticity. The VMC does not make many assumptions on the system that hosts its graph. Thus, in principle, it can be implemented in various types of systems, with different sensors and connectivity options as well as and environmental interactions.

7 Conclusion

In this paper, we presented theoretical, numerical, and physical experimental studies of some of the dynamic and structural behaviors of VMC. The knowledge gained from these studies facilitates the process of choosing parameters for different applications of VMC according to various requirements of the given tasks. VMC is a dynamic transportation network consisting of agents that collectively decide which paths to expand further or to shrink by taking into account the given environment. The investigations of the dynamics indicate an intrinsic tendency of VMC to favor shorter paths. They also demonstrate the tunable tendency of VMC for exploration, exploitation, or sticking to old decisions. Furthermore, the parameter study revealed a critical effect of the transfer rate of successin, which is a parameter influencing information transfer (discussed in Sect. 6). The study showed a transition from instability to stability and an explosion of the network size at the critical value of the transfer rate.

In VMC, a collective of agents control the distribution of a shared resource among itself, and this distribution, in turn, affects the organization of the collective. Here we have pointed to the similarity between the diagram of decision making performance against the amount of shared resource in the VMC (Fig. 15) and the generic diagram of system performance versus system size in collective robotic systems. We also discussed parallels between VMC and

other collective systems in terms of resource distribution, transportation networks, collective decision making, and feedback loops (Sect. 6). In general, similarities are shared across different types of natural and artificial systems, from animal collectives, through vascular and neural networks, to traffic systems and collective robotics. Such a unified viewpoint paves the way for a deeper understanding of these systems and exploring alternative methods to design artificial systems, e.g., novel types of artificial neural networks or collective decision making systems. By presenting evidence on similarities between VMC and various other systems, this paper suggests potential benefits of approaching these systems from a shared viewpoint, which is collective resource distribution.

References

Bebber, D. P., Hynes, J., Darrah, P. R., Boddy, L., & Fricker, M. D. (2007). Biological solutions to transport network design. *Proceedings of the Royal Society B: Biological Sciences*, *274*(1623), 2307–2315.

Bejan, A., & Zane, J. (2012). *Design in nature: How the constructal law governs evolution in biology, physics, technology, and social organization*. New York: Doubleday.

Bennett, T., Hines, G., & Leyser, O. (2014). Canalization: What the flux? *Trends in Genetics*, *30*(2), 41–48.

Bonabeau, E., Dorigo, M., & Theraulaz, G. (1999). *Swarm intelligence: From natural to artificial systems*. Oxford: Oxford Univ. Press.

Bonabeau, E., Sobkowski, A., Theraulaz, G., & Deneubourg, J. L. (1997). Adaptive task allocation inspired by a model of division of labor in social insects. In *Biocomputing and emergent computation: Proceedings of BCEC97* (pp. 36–45). World Scientific Press.

Camazine, S., Deneubourg, J. L., Franks, N. R., Sneyd, J., Theraulaz, G., & Bonabeau, E. (2001). *Self-organizing biological systems*. Princeton: Princeton Univ. Press.

Campo, A., Gutiérrez, Á., Nouyan, S., Pinciroli, C., Longchamp, V., Garnier, S., et al. (2010). Artificial pheromone for path selection by a foraging swarm of robots. *Biological Cybernetics*, *103*(5), 339–352.

Clearwater, S. H. (Ed.). (1996). *Market-based control: A paradigm for distributed resource allocation*. River Edge: World Scientific Publishing Co., Inc.

Crawford, S., Shinohara, N., Sieberer, T., Williamson, L., George, G., Hepworth, J., et al. (2010). Strigolactones enhance competition between shoot branches by dampening auxin transport. *Development*, *137*(17), 2905–2913.

Deconinck, G., Craemer, K. D., & Claessens, B. (2015). Combining market-based control with distribution grid constraints when coordinating electric vehicle charging. *Engineering*, *1*(4), 453–465.

Detrain, C., & Deneubourg, J. L. (2006). Self-organized structures in a superorganism: Do ants behave like molecules? *Physics of Life Reviews*, *3*(3), 162–187.

Devert, A., Bredeche, N., & Schoenauer, M. (2011). Robustness and the halting problem for multicellular artificial ontogeny. *IEEE Transactions on Evolutionary Computation*, *15*(3), 387–404.

Divband S. M., Ghofrani, J., Zahadat, P., & Hamann, H. (2018a). Robust and adaptive robot self-assembly based on vascular morphogenesis. In *International conference on intelligent robots*. (in press).

Divband S. M., Zahadat, P., Ghofrani, J., & Hamann, H. (2018b). Adaptive path formation in self-assembling robot swarms by tree-like vascular morphogenesis. In *Conference: 2018 international symposium on distributed autonomous robotic systems (DARS)*. (in press).

Domagalska, M. A., & Leyser, O. (2011). Signal integration in the control of shoot branching. *Nature Reviews Molecular Cell Biology*, *12*, 211.

Dorigo, M., Birattari, M., & Brambilla, M. (2014). Swarm robotics. *Scholarpedia*, *9*(1), 1463. revision #138643.

Dorigo, M., Maniezzo, V., & Colorni, A. (1996). Ant system: Optimization by a colony of cooperating agents. *IEEE Transactions on Systems, Man, and Cybernetics, Part B, 26*(1), 29–41.

dos Silva, S., Viana, R. F., & Lopes, S. (2015). Pattern formation and turing instability in an activator-inhibitor system with power-law coupling. *Physica A: Statistical Mechanics and its Applications*, *419*, 487–497.

Doursat, R., Sánchez, C., Dordea, R., Fourquet, D., & Kowaliw, T. (2012). Embryomorphic engineering: Emergent innovation through evolutionary development. In R. Doursat, H. Sayama, & O. Michel (Eds.), *Morphogenetic Engineering* (pp. 275–311). Springer, Berlin Heidelberg: Understanding Complex Systems.

Franks, N. R., Mallon, E. B., Bray, H. E., Hamilton, M. J., & Mischler, T. C. (2003). Strategies for choosing between alternatives with different attributes: Exemplified by house-hunting ants. *Animal Behaviour*, *65*(1), 215–223.

Goodwin, B. (2001). *How the leopard changed its spots: The evolution of complexity*. Princeton: Princeton Univ Press.

Halloy, J., Sempo, G., Caprari, G., Rivault, C., Asadpour, M., Tâche, F., et al. (2007). Social integration of robots into groups of cockroaches to control self-organized choices. *Science*, *318*(5853), 1155–1158.

Hamann, H. (2018a). Superlinear scalability in parallel computing and multi-robot systems: Shared resources, collaboration, and network topology. In *Architecture of computing systems—ARCS 2018—31st international conference, Braunschweig, Germany, April 9–12, 2018, Proceedings* (pp. 31–42).

Hamann, H. (2018b). *Swarm robotics: A formal approach*. Berlin: Springer.

Hamann, H., Soorati, M., Heinrich, M., Hofstadler, D., Kuksin, I., Veenstra, F., Wahby, M., Nielsen, S., Risi, S., Skrzypczak, T., Zahadat, P., Wojtaszek, P., StÃžy, K., Schmickl, T., Kernbach, S., & Phil, A. (2017). flora robotica—An architectural system combining living natural plants and distributed robots. arXiv preprint arXiv:1709.04291

Heinrich, M. K., Zahadat, P., Harding, J., & Brandt, M. N., et. al (2018). Using interactive evolution to design behaviors for non-deterministic self-organized construction. In *Symposium on simulation for architecture and urban design (SimAUD)*.

Hofstadler, D. N., Varughese, J. C., Nielsen, S. A., Leon, D. A., Ayres, P., Zahadat, P., & Schmickl, T. (2018). Artificial plants—Vascular morphogenesis controller-guided growth of braided structures. arXiv preprint arXiv:1804.06343.

Hornby, G. S., & Pollack, J. B. (2001). Body-brain co-evolution using L-systems as a generative encoding. In *Proceedings of the genetic and evolutionary computation conference (GECCO-2001)* (pp. 868–875). Morgan Kaufmann, San Francisco, California, USA.

Huberman, B. A., & Hogg, T. (1995). Distributed computation as an economic system. *Journal of Economic Perspectives*, *9*(1), 141–152.

Karsai, I., & Schmickl, T. (2011). Regulation of task partitioning by a "common stomach": A model of nest construction in social wasps. *Behavioral Ecology*, *22*, 819–830.

Kebrom, T. H. (2017). A growing stem inhibits bud outgrowth—The overlooked theory of apical dominance. *Frontiers in Plant Science*, *8*(October), 1–7.

Kowaliw, T., & Banzhaf, W. (2012). *Mechanisms for complex systems engineering through artificial development* (pp. 331–351). Berlin Heidelberg: Springer.

Kurose, J. F., & Simha, R. (1989). A microeconomic approach to optimal resource allocation in distributed computer systems. *IEEE Transactions on Computers*, *38*(5), 705–717.

Laschi, C., & Mazzolai, B. (2016). Lessons from animals and plants: The symbiosis of morphological computation and soft robotics. *IEEE Robotics Automation Magazine*, *23*(3), 107–114.

Leyser, O. (2011). Auxin, self-organisation, and the colonial nature of plants. *Current Biology*, *21*(9), R331–R337.

Lindenmayer, A. (1975). Developmental algorithms for multicellular organisms: A survey of L-systems. *Journal of Theoretical Biology*, *54*(1), 3–22.

Lucas, W. J., Groover, A., Lichtenberger, R., Furuta, K., Yadav, S. R., Helariutta, Y., et al. (2013). The plant vascular system: Evolution, development and functions. *Journal of Integrative Plant Biology*, *55*(4), 294–388.

Ma, Q., Johansson, A., Tero, A., Nakagaki, T., & Sumpter, D. J. T. (2013). Current-reinforced random walks for constructing transport networks. *Journal of The Royal Society Interface*, *10*(80), 20120864.

Meng, Y., Guo, H., & Jin, Y. (2013). A morphogenetic approach to flexible and robust shape formation for swarm robotic systems. *Robotics and Autonomous Systems*, *61*(1), 25–38.

Morris, E. C., Griffiths, M., Golebiowska, A., Mairhofer, S., Burr-Hersey, J., Goh, T., et al. (2017). Shaping 3d root system architecture. *Current Biology*, *27*(17), R919–R930.

Murray, J. D. (2003). On the mechanochemical theory of biological pattern formation with application to vasculogenesis. *Comptes Rendus Biologies*, *326*(2), 239–252.

Nakagaki, T., Yamada, H., & Toth, A. (2000). Maze-solving by an amoeboid organism. *Nature*, *407*, 470–470.

O'Grady, R., Christensen, A. L., & Dorigo, M. (2012). *SWARMORPH: Morphogenesis with self-assembling robots* (pp. 27–60). Berlin, Heidelberg: Springer.

Payton, D., Daily, M., Estowski, R., Howard, M., & Lee, C. (2001). Pheromone robotics. *Autonomous Robots*, *11*(3), 319–324.

Perna, A., Granovskiy, B., Garnier, S., Nicolis, S. C., Labédan, M., Theraulaz, G., et al. (2012). Individual rules for trail pattern formation in argentine ants (linepithema humile). *PLOS Computational Biology*, *8*(7), 1–12.

Pini, G., Brutschy, A., Pinciroli, C., Dorigo, M., & Birattari, M. (2013). Autonomous task partitioning in robot foraging: An approach based on cost estimation. *Adaptive Behavior*, *21*(2), 117–135.

Rubenstein, M., Cornejo, A., & Nagpal, R. (2014). Programmable self-assembly in a thousand-robot swarm. *Science*, *345*(6198), 795–799.

Sachs, T. (1981). The control of the patterned differentiation of vascular tissues. *Advances in Botanical Research*, *9*, 151–262.

Sachs, T. (2004). Self-organization of tree form: A model for complex social systems. *Journal of Theoretical Biology*, *230*(2), 197–202.

Sachs, T. (2006). How can plants choose the most promising organs? In F. Baluška, S. Mancuso, & D. Volkmann (Eds.), *Communication in plants: Neuronal aspects of plant life, chap. 4* (pp. 53–63). Berlin Heidelberg: Springer.

Seeley, T. D., & Buhrman, S. C. (2001). Nest-site selection in honey bees: How well do swarms implement the "best-of-n" decision rule? *Behavioral Ecology and Sociobiology*, *49*(5), 416–427.

Sims, K. (1994). Evolving 3D morphology and behavior by competition. In R. Brooks & P. Maes (Eds.), *Artificial Life IV* (pp. 28–39). Cambridge: MIT Press.

Slater, D. (2018). Natural bracing in trees: Management recommendations. *Arboricultural Journal*, *40*(2), 106–133.

Slavkov, I., Carrillo-Zapata, D., Carranza, N., Diego, X., Jansson, F., Kaandorp, J., et al. (2018). Morphogenesis in robot swarms. *Science Robotics*, *3*(25), eaau9178.

Sperati, V., Trianni, V., & Nolfi, S. (2011). Self-organised path formation in a swarm of robots. *Swarm Intelligence*, *5*(2), 97–119.

Stoy, K., & Nagpal, R. (2007). Self-reconfiguration using directed growth. In R. Alami, R. Chatila, & H. Asama (Eds.), *Distributed autonomous robotic systems 6* (pp. 3–12). Tokyo: Springer Japan.

Sumpter, D. (2006). The principles of collective animal behavior. *Philosophical Transactions of the Royal Society of London. Series B, Biological sciences*, *361*, 5–22.

Szopek, M., Schmickl, T., Thenius, R., Radspieler, G., & Crailsheim, K. (2013). Dynamics of collective decision making of honeybees in complex temperature fields. *PLoS ONE*, *8*(10), 1–11.

Turing, A. M. (1952). The chemical basis of morphogenesis. *Philosophical Transactions of the Royal Society of London. Series B, Biological Sciences*, *B237*(641), 37–72.

Waldspurger, C. A., Hogg, T., Huberman, B. A., Kephart, J. O., & Stornetta, S. (1992). Spawn: A distributed computational economy. *IEEE Transactions on Software Engineering*, *18*(2), 103–117.

Zahadat, P. (2019). Self-adaptation and self-healing behaviors via a dynamic distribution process. In *2019 IEEE 13th international conference on self-adaptive and self-organizing systems (SASO)*. IEEE.

Zahadat, P., Hahshold, S., Thenius, R., Crailsheim, K., & Schmickl, T. (2015). From honeybees to robots and back: Division of labor based on partitioning social inhibition. *Bioinspiration and Biomimetics*, *10*(6), 066005.

Zahadat, P., Hofstadler, D. N., & Schmickl, T. (2017a). Development of morphology based on resource distribution: Finding the shortest path in a maze by vascular morphogenesis controller. In *14th European conference on artificial life (ECAL-2017)* (vol. 14, pp. 428–429).

Zahadat, P., Hofstadler, D. N., & Schmickl, T. (2017b). Vascular morphogenesis controller: A generative model for developing morphology of artificial structures. In *Proceedings of the genetic and evolutionary computation conference* (pp. 163–170). GECCO '17, New York: ACM.

Zahadat, P., Hofstadler, D. N., & Schmickl, T. (2018). Morphogenesis as a collective decision of agents competing for limited resource: A plants approach. In M. Dorigo, M. Birattari, C. Blum, A. L. Christensen, A. Reina, & V. Trianni (Eds.), *Swarm Intelligence. Lecture Notes in Computer Science* (Vol. 11172, pp. 84–96).

Zahadat, P., & Schmickl, T. (2014). Generation of diversity in a reaction–diffusion-based controller. *Artificial Life*, *20*(3), 319–342.

Zahadat, P., & Schmickl, T. (2016). Division of labor in a swarm of autonomous underwater robots by improved partitioning social inhibition. *Adaptive Behavior*, *24*(2), 87–101.

Zahadat, P., & Schmickl, T. (2017). Evolving vascular morphogenesis controller to demonstrate locomotion. In *2017 Artificial intelligence and signal processing conference (AISP)* (pp. 352–357).

Zahadat, P., & Schmickl, T. (2018). Locomotion as a result of displacement of resources. In *The 2018 conference on artificial life: A hybrid of the european conference on artificial life (ECAL) and the international conference on the synthesis and simulation of living systems (ALIFE)* (pp. 232–233).

Publisher's Note Springer Nature remains neutral with regard to jurisdictional claims in published maps and institutional affiliations.